Functional imaging and quantification of multi-neuronal olfactory responses in *C. elegans*

Albert Lin[1,3,✉], **Shanshan Qin**[2,3], **Helena Casademunt**[1,3], **Min Wu**[5], **Wesley Hung**[5], **Greg Cain**[1], **Nicolas Z. Tan**[4], **Raymond Valenzuela**[4], **Leila Lesanpezeshki**[5], **Cengiz Pehlevan**[2,3], **Vivek Venkatachalam**[4], **Mei Zhen**[*5], **and Aravinthan D.T. Samuel**[*1,3,✉]

[1]Department of Physics, Harvard University, Cambridge, MA, USA
[2]John A. Paulson School of Engineering and Applied Sciences, Harvard University, Cambridge, MA, USA
[3]Center for Brain Science, Harvard University, Cambridge, MA, USA
[4]Department of Physics, Northeastern University, Boston, MA, USA
[5]Lunenfeld-Tanenbaum Research Institute, Mount Sinai Hospital, Toronto, ON, Canada
[*] *These authors share senior authorship*

Abstract

Many animals perceive odorant molecules by collecting information from ensembles of olfactory neurons. These neurons employ receptors that are tuned to recognize odorant molecules by chemical binding affinity. Olfactory systems are able, in principle, to detect and discriminate large numbers of odorants by using combinatorial coding strategies. Multineuronal imaging, combined with high-throughput stimulus delivery, allow for the comprehensive measurement of ensemble-level sensory representations. Here, we used microfluidics and multineuronal imaging to study olfactory representations at the sensory periphery of the nematode *C. elegans*. The collective activity of chemosensory neurons in *C. elegans* reveals high-dimensional representations of olfactory information across a broad space of odorant molecules. We reveal diverse tuning properties and dose-response curves across chemosensory neurons and across odorant molecules. We describe the unique contribution of each sensory neuron to an ensemble-level olfactory code, and show how the encoding of a set of natural stimuli, nematode pheromones, differs from the encoding of small volatile organic molecules. The integrated activity of the sensory periphery of *C. elegans* contains sufficient information to robustly encode the intensity and identity of a broad panel of odorants.

C. elegans | multi-neuronal imaging | chemosensation | odor representation
Correspondence: *albertlin@g.harvard.edu*
Correspondence: *samuel@g.harvard.edu*

Introduction

Many animals exhibit diverse behaviors – navigating the world, finding food, and avoiding dangers – on the basis of a wide range of olfactory cues. To do this, their olfactory systems must distinguish the identity and intensity of many chemically diverse odorant molecules. The olfactory systems of insects and mammals have large ensembles of olfactory sensory neurons (1–6). Each olfactory sensory neuron usually expresses a specific olfactory receptor that confers the neuron's sensitivity to odorant molecules. Each olfactory receptor is tuned to recognize odorant molecules by chemical binding affinity (7). A given receptor is typically activated by many different odorant molecules, each to varying degree reflecting differences in chemical affinity. A given odorant molecule also typically activates multiple olfactory receptors to varying degrees (1, 8). A distribution of olfactory receptors with affinities for different molecules allows the system as a whole to detect and discriminate a large variety of odorant molecules. Olfactory recognition through the collective activity of ensembles of olfactory neurons is suggestive of combinatorial coding strategies.

Combinatorial codes allow small numbers of olfactory sensory neurons to encode much larger numbers of olfactory stimuli. In insects and mammals, information from olfactory sensory neuron ensembles is integrated by the next downstream layers – the antennal lobe in insects and the olfactory bulb in mammals – in a largely feed-forward manner (9, 10). The antennal lobe and olfactory bulb integrate the activity of all olfactory sensory neurons, and pass this information to higher processing centers for innate and learned behaviors. The cellular and synaptic organization of these first layers of olfactory processing is broadly similar in insects and mammals (11–13). In insects and mammals, higher brain centers for diverse olfactory behaviors use information that is first processed by their olfactory sensory neuron ensembles (14–18).

Olfaction is an essential sensory modality for many behaviors in the nematode *C. elegans* (19, 20). However, the neural circuits for olfactory behavior in *C. elegans* have a very different cellular and molecular layout compared to larger animals. The *C. elegans* genome encodes more than 1000 putative chemosensory GPCR receptors, suggesting a substantial capacity for detecting odorant molecules (21, 22). However, the nematode's large family of receptors is expressed in a small nervous system with only 11 pairs of amphid chemosensory neurons (21, 23). Each chemosensory neuron expresses multiple types of olfactory receptors, and many chemosensory neurons are polymodal, having receptors for other modalities. In addition to sensing volatile odorant molecules, polymodal chemosensory neurons detect other soluble chemicals (pheromones, salts, amino acids), gases (CO_2, O_2), and temperature (21, 24). The anatomical wiring diagram of *C. elegans* indicates that, unlike in insects and mammals, some chemosensory neurons are directly wired together and receive direct synaptic feedback from interneurons that integrate olfactory information from other chemosensory neurons (25, 26) (**Figure 1A**). Also unlike larger animals, chemosensory neurons in *C. elegans* synapse in different ways onto interneurons for different behaviors. For example, the ASH chemosensory neuron is a nociceptive neuron. The AVA, AVB, and AVD command motor interneurons for forward and backward movement receive more direct synaptic input from ASH than from any other chemosensory neuron (27–30). This pattern of synaptic connectivity is compatible with mediating

rapid innate reflexive avoidance behavior to stimuli that activate ASH, including the portion of olfactory space associated with repulsive odorant molecules. The AIA, AIB, AIY, and AIZ interneurons play roles in goal-directed locomotion and learning behaviors (31–34). These interneurons broadly integrate information from all chemosensory neurons, suggesting a capacity for navigation and olfactory plasticity that spans the full space of odorant molecules.

Many studies have probed the detection of small sets of odorant molecules by individual chemosensory neurons in *C. elegans* (35–41). Isoamyl alcohol is detected by AWC, AWB, and ASH (35). Diacetyl is detected by AWA at low concentrations and by ASH at high concentrations (36). Benzaldehyde is detected by by AWA, AWB, AWC, and ASE (37). In some cases, the left and right pairs of a chemosensory neuron type detect different odorant molecules. AWCL and AWCR are stochastically asymmetric. In each worm, one neuron (either AWCL or AWCR) adopts the identity AWC^{ON} and its lateral pair adopts the identity AWC^{OFF} (40). AWC^{ON} detects butanone, while AWC^{OFF} detects 2,3-pentanedione (32, 42). The gustatory ASEL and ASER neurons represent another chemosensory pair with lateralized sensitivity, responding asymmetrically to different ions during salt chemotaxis – ASEL detects sodium ions, and ASER detects chloride and potassium ions (43, 44). Behavioral experiments have identified many more odorants which are attractive or repulsive to the worm (45, 46). We now have a rich understanding of the odor response properties of individual chemosensory neurons in *C. elegans*, but how the chemosensory neuron ensemble collectively encodes the full range of diverse olfactory stimuli remains largely unknown.

We set out to characterize how the activity of the entire chemosensory neuron ensemble in *C. elegans* encodes a chemically diverse space of volatile odorant molecules. We sought to quantify chemosensory neuron responses to different molecules with a broad range of chemical structures. We assembled a panel of olfactory stimuli spanning a diverse chemistry of odorant molecules and used microfluidics to deliver these olfactory stimuli at multiple concentrations in a controlled manner to each animal (**Figure 1B**). To efficiently record neuronal response patterns throughout the *C. elegans* sensory periphery, we used a transgenic animal that allowed the simultaneous measurement of intracellular calcium dynamics in all eleven pairs of amphid chemosensory neurons using volumetric imaging (**Figure 1C**).

We found that odor-evoked responses for most odorant molecules are widespread across the sensory periphery. Single neuron detection of particular odorant molecules is rare, while collective neuronal responses are common. Dose-response curves are different for different odorant molecules, whether comparing the responses of the same neuron to different odorants or comparing the responses of different neurons to the same odorant. Odor identity and intensity information can be reliably decoded by the collective odor-evoked activity of the entire chemosensory periphery. Analyzing mutants lacking synaptic transmission, we found that odor representations at the chemosensory layer are largely independent of synaptic connections. We also characterized the chemosensory representations of a set of *C. elegans* pheromones, and found that these representations differ from those of volatile odorants. The small nervous system of *C. elegans* thus has the capacity to use ensemble-level representations of olfactory cues to robustly discriminate the identity and intensity of odorant molecules across olfactory stimulus space.

Results

Labeling and recording from chemosensory neurons

We developed a transgenic animal (ZM10104) to simultaneously identify and record calcium dynamics in all 11 pairs of amphid chemosensory neurons in *C. elegans*: AWA, AWB, AWC, ASE, ASG, ASH, ASI, ASJ, ASK, ADL, and ADF (**Figure 1A**) (21). To image calcium dynamics, we drove expression of GCaMP6s in all ciliated sensory neurons under the control of the *ift-20* promoter (47). We localized GCaMP6s expression to cellular nuclei to make it easier to segment signals from separate neurons. To identify neurons on the basis of morphology and relative position, we also expressed wCherry under the control of the *gpc-1* promoter that labels a sparse subset of chemosensory neurons (AWB, AWC, ASH, ASE, ASI, and ASJ) (**Figure 1C, Appendix A**).

We implemented the controlled delivery of odor solutions with a multichannel microfluidic device. This device was adapted from an original design to study olfactory representations to diverse odorants in the *Drosophila* larva (4). Here, young adult *C. elegans* were immobilized and positioned to allow odorants in a delivery channel to flow past the animal's nose (**Figure 1B**) (48). Neuronal calcium activity was captured with volumetric imaging at 2.5Hz with a spinning disk confocal microscope (**Figure 1D**).

Odor identities are encoded by ensemble activity

We assembled a stimulus panel of 23 odorant molecules. This panel was selected from 122 molecules that had previously been used to study *C. elegans* olfaction (45, 46). The 23 odorant molecules were chosen to span the chemical diversity of previously studied stimuli. The panel contains exemplars from six chemical classes: alcohols, aromatics, esters, ketones, pyrazines, and thiazoles. To assess chemical diversity, we constructed an odor space of known *C. elegans* olfactory stimuli on the basis of physical and chemical descriptors of molecular structure (49). Our 23 odorants represent a broad sampling of this geometrical space (**Figure S3A**) (49). We recorded the responses of the 11 pairs of chemosensory neurons in *C. elegans* to over 70 stimulus conditions, testing each of the 23 odorants at multiple concentrations. Individual animals were repeatedly presented with series of 10s odorant pulses separated by 30s buffer blanks. For each stimulus condition, we recorded the responses to an average of 100 odor presentations across multiple animals (**Figure 2A-C, S3C-D**).

Across our odorant panel, we were largely able to reproduce known olfactory responses of sensory neurons to stimuli. For example, we confirmed that the AWA neuron reliably detects diacetyl from low concentrations (10^{-6} dilution) to high concentrations (10^{-4} dilution). AWA exhibits an increase in intracellular calcium upon odor onset, an 'ON response' (50). However, we also found that every odorant reliably activated more

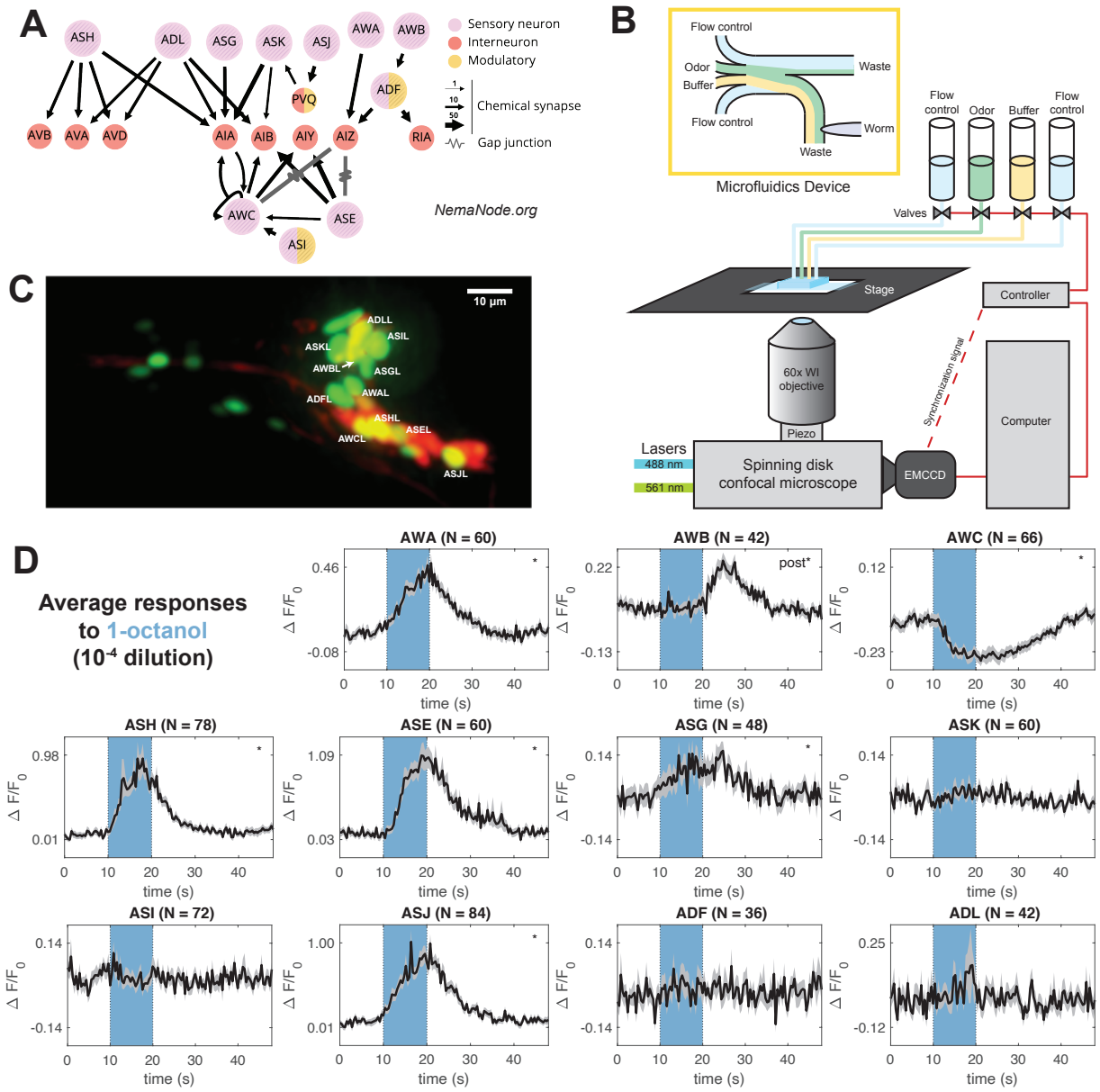

Figure 1. Labeling and recording from the chemosensory neurons. (A) Downstream partners of the 11 chemosensory neurons identified in the *C. elegans* connectome (25, 26). Panel generated at nemanode.org. **(B)** Adult *C. elegans* were immobilized inside a microfluidic device and presented with odor solutions in a highly controlled manner. Each animal was volumetrically imaged at 2.5 Hz with a spinning disk confocal microscope during odor presentations. **(C)** The animals expressed nuclear-localized GCaMP6s in all ciliated sensory neurons. A sparse wCherry landmark allowed us to identify the 11 chemosensory neurons. Seen here is a dual-color maximum projection image of the head of the worm. The 11 chemosensory neurons on the near (L) side are labeled in the figure. For clarity, the chemosensory neurons on the far side of the animal and other ciliated neurons are unlabeled. **(D)** Neuronal activity traces of the 11 chemosensory neurons in response to a single odorant condition (1-octanol, 10^{-4} dilution), averaged across trials. The 10 second odorant delivery period is indicated by the colored bar. Significant responses ($q \leq 0.01$) are marked with stars, with "post" indicating a significant response to stimulus removal (OFF response). Error bars (gray) are the standard error of the mean.

sensory neurons than previously described. For example, we discovered that ASJ is reliably activated by 1-octanol, a novel ON response. We also discovered that AWC reliably detects diacetyl at low concentrations, but with a decrease in intracellular calcium upon odor onset.

Similarly for isoamyl alcohol, another well-studied odorant, we were able to both reproduce known responses and discover new responses. Previous calcium imaging experiments showed that the AWA, AWB, and AWC neurons are most sensitive to isoamyl alcohol, whereas the ASH neuron is only activated by isoamyl alcohol at high concentrations (35). We confirmed these known responses, and identified novel responses to isoamyl alcohol in the ASE and ASG neurons (**Figure 2A-C**).

Most of the chemosensory neurons exhibited ON responses to most odorants. However, we also observed OFF responses, where calcium levels change upon odorant removal. Some chemosensory neurons exhibited ON responses to some odorants and OFF responses to other odorants. For example, the AWB neuron is activated upon the removal of odorants such as 1-octanol, but activated by the onset of other odorants, such as diacetyl and isoamyl alcohol at high concentration (**Figure 1D**). AWB has previously been reported to exhibit ON and OFF

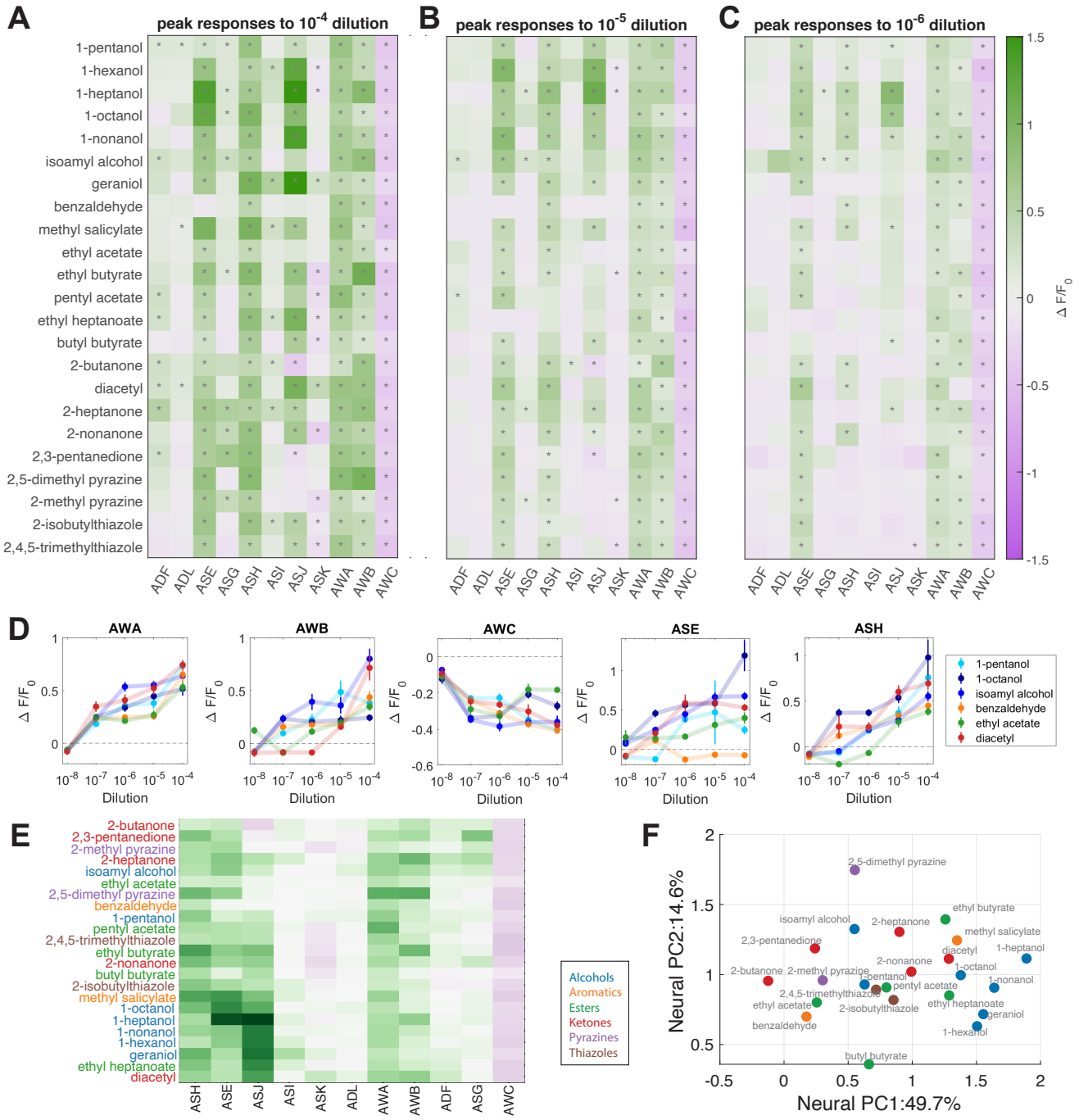

Figure 2. Ensemble responses to a broad panel of odorants. Average peak responses of the 11 chemosensory neurons to odorants at **(A)** high concentration (10^{-4} dilution), **(B)** medium concentration (10^{-5} dilution), and **(C)** low concentration (10^{-6} dilution). Peaks were computed from a time window from the onset of odor delivery to 10 s after odor removal. Responses are reported as $\Delta F/F_0$, and significant responses ($q \leq 0.01$, 2-tailed, paired t-tests) are indicated with stars. Most odorants elicit significant responses from unique combinations of neurons. **(D)** Dose responses of the peak responses of AWA, AWB, AWC, ASE, and ASH are diverse, with distinct concentration-dependent curves in response to different odorants. Refer to **Figure S3F** for the dose responses of the other 6 sensory neurons. Error bars are standard error of the mean. **(E)** Odorants (high concentration) clustered by their peak average neuronal responses. **(F)** A PC space built from standardized peak average neural responses. Chemical class is indicated by color. In both representations of neural space, we see that some groups of classes of odorants, such as alcohols and ketones, have more similar neural representations, while other classes of odorants, such as esters, have more diverse representations. Refer to **Figure S3G** for PC loadings.

responses to different concentrations of isoamyl alcohol (35) (**Figure S2A**).

Previous work showed that AWC is inhibited by several odorants in our assay, including diacetyl, benzaldehyde, and 2-butanone (34, 36, 37, 41). We found that AWC is inhibited by every odorant in our panel (**Figure 2A**). We also discovered that ASK has inhibitory responses to many odorants including ethyl butyrate and 2-nonanone (**Figure S2B**). Some neurons exhibited inhibitory response to certain odorants but excitatory responses to others. For example, ASJ has a strong inhibitory response to 2-butanone but a strong excitatory response to 1-nonanol (**Figure S2C**).

The left and right ASE and AWC neurons are known to be asymmetrically activated by specific chemical stimuli (40, 44). Two odorants in our panel – heptanoate and butyl butyrate – evoked asymmetric responses in the ASEL and ASER neurons (**Figure S2D**). Whereas the cellular identities of ASEL and ASER are defined by their handedness, the AWCL and AWCR neurons stochastically adopt the identities of AWC^{ON} or AWC^{OFF} (AWC^{ON} can be identified via cell-specific expression of the *str-2* promoter). In our experiments, we cannot distinguish which AWC neuron is AWC^{ON} or AWC^{OFF}, except by inference from neuronal activity patterns. Because the left and right sensory neurons of all other types respond symmetrically to all odorants, and because the left and right ASE and AWC neurons also respond symmetrically to many odorants, we grouped the signals from left and right sensory neurons in all analyses unless otherwise noted.

At high concentrations, every odorant that we studied activated multiple sensory neurons. Across odorants, we observed significant overlap in each set of responding neurons. AWA, AWB, and AWC were the most broadly tuned neurons, significantly responding to most of the odorant panel.

One method of representing the temporal dynamics of the eleven sensory neurons in response to a given odorant is to compute cross-correlations in the activities of every neuron pair. We found that these matrices of pairwise cross-correlations are distinct for different odorants (**Figure S4A-B**).

From both the peak responses and the dynamics, we see that the diversity of ensemble-level dynamics is as large as the number of odorants tested. *C. elegans* may encode the identities of a large number of odorants by using the combinatorially large space of distinct activity patterns that can be exhibited by a small number of sensory neurons.

Olfactory representations broaden with increasing concentrations

We measured the dose-response curve of every odorant across all sensory neurons, measuring the peak responses to each odorant over 3-5 orders of magnitude in concentration (**Figure 2A-C, S3C-D**). The highest tested concentration for any odorant was at 10^{-4} dilution. At 10^{-8} dilution, all tested odorants were below detection threshold for all sensory neurons. For most odorants and neurons, response magnitudes exhibited a monotonic increase with odorant concentration. When neurons were activated at low concentrations, they were also activated at all higher concentrations. Thus, every odorant is associated with a characteristic set of neurons that is activated at all concentrations above the detection threshold. For example, at all concentrations that we observed sensory responses for 1-pentanol, AWA and AWC were activated. At all concentrations that we observed sensory responses for 1-octanol, ASE, ASH, AWA, AWB, and AWC were activated. At all concentrations that benzaldehyde was detected, AWA, AWB, and AWC were activated. Because of the stability of the characteristic set of neurons that are activated at different odorant concentrations above threshold, the set of activated neurons can be taken as a unique olfactory representation signifying the identity of each odorant.

For many odorants, increasing intensity also spatially broadens olfactory representation by activating additional sensory neurons. This happens because different sensory neurons exhibit different thresholds for different odorants. For example, AWB is only activated by 1-pentanol at concentrations above 10^{-5} dilution, and ADF, ADL, and ASG become significantly activated by 1-pentanol only at the highest tested concentration (**Figure S3E**). Thus, odorant intensity is partly in the magnitude of the responses of activated neurons and partly encoded in the spatial breadth of activated neurons.

We employed phase-trajectory analysis to illustrate the joint encoding of odorant intensity and identity in ensemble-level representation. We used principal component analysis to better understand the ensemble-level representation of odorants delivered at different intensities over time following odorant onset and removal. In a low-dimensional principal component space, these ensemble-level representations follow closed trajectories that start and end at baseline activity (**Figure S4C**). Along each trajectory, neurons become activated at odorant onset, reach their peak responses, and recover to baseline after odorant removal. In this principal component space, the trajectory that corresponds to the response to a given odorant has a specific direction away from the origin. The segregation of olfactory representations for different odorants is signified by different directions of these trajectories in principal component space. Trajectories for responses to the same odorant at different intensities are aligned in direction but differ in magnitude in principal component space.

Diverse dose responses across neurons and odorants

We constructed dose-response curves for all 11 sensory neurons in response to the odorants in the panel. We uncovered a diversity of dose-response curves that differed in threshold and steepness of response magnitude as a function of odorant concentration (**Figure 2D, S3F**). We found that a given odorant can evoke dose-response curves with different steepness and threshold in different neurons. At the same time, each sensory neuron can exhibit dose-response curves with different steepness and threshold for different odorants. In some cases, sensory neurons detected an odorant with slowly graded responses over a broad dynamic range. Examples of slowly graded curves include the AWA dose-response to 1-pentanol and the AWB dose-response to 1-heptanol (**Figure 2D, S3F**). In other cases, sensory neurons exhibited steep response functions, becoming fully activated or fully inhibited above a sharply defined threshold. Examples of step-like curves include the ASE dose-response to 1-pentanol

and the AWB dose-response to 1-octanol.

In insects and mammals, olfactory receptor neurons typically have similar dose-response curves across neurons and odorants (4, 51, 52). The difference in dose-response curves between larger animals and *C. elegans* may arise from the difference between olfactory systems where sensory neurons are equipped with one receptor type (each with a specific threshold for each odorant as in insects and mammals) versus an olfactory system where each neuron expresses multiple receptors and each receptor has a different threshold for each odorant. When neurons express one receptor type, the overall cellular response can be fit to one activation curve with one odorant-dependent free variable (the receptor-ligand binding constant). In the *Drosophila* larva, for example, every dose-response curve for every neuron and every odorant follows one functional form after alignment to the odorant concentration that evokes half-maximal activity (4). *C. elegans* sensory neurons, because they express many receptors with different thresholds for a given odorant, can exhibit graded responses over a broad dynamic range. As additional receptor types with higher thresholds are recruited at higher concentrations, a sensory neuron can become cumulatively more active.

The best characterized olfactory receptor in *C. elegans* is ODR-10 that is expressed by AWA and is highly sensitive to diacetyl (50, 53). It is known that AWA responds to many other odorants in a manner that is independent of ODR-10, direct evidence that AWA expresses multiple receptors (35–37, 45). Other sensory neurons that do not express ODR-10 are activated by diacetyl at higher threshold concentrations. Without a comprehensive characterization of the repertoire of functional receptors that are used by each type of sensory neuron in *C. elegans*, it is difficult to quantitatively extract the molecular parameters of each receptor-ligand interaction from dose-response curves in thge worm, as has been done in *Drosophila* and other systems (4, 54, 55).

ASH dose-responses curves are correlated with behavioral valence

In previous behavioral experiments, most odorants in our panel were shown to be attractive at low concentrations and aversive at high concentrations. A few odorants – such as 1-heptanol, 1-octanol, and 1-nonanol – are aversive at any tested concentration (**Appendix B**).

The nociceptive ASH sensory neuron mediates the behavioral response to several aversive stimuli (27–30). We found that every odorant in our panel elicits strong ASH responses when presented at high concentration (**Figure 2A**). We also found that odorants to which ASH is most sensitive are those odorants that are aversive at all concentrations. For example, 1-octanol and 1-nonanol elicit larger responses in ASH at lower concentrations than attractive odorants such as hexanol or isoamyl alcohol. No other sensory neuron is specifically most sensitive to the most aversive odorants in our panel. Unique among chemosensory neurons, ASH has direct synaptic connections to command motor interneurons for forward and backward movement (AVA, AVB, and AVD) (25, 26, 56). Thus, ASH appears to be part of a reflex arc that directly encodes behavioral valence by triggering reversal movements upon odorant detection.

Comparing ensemble-level representations of odorants

Across odorants, we observed significant overlap in the corresponding sets of activated neurons. Quantitative differences in the sensitivity of sensory neurons to odorants will depend on cell-specific patterns of expression of olfactory receptors. In most olfactory systems, a typical olfactory receptor is activated by a range of structurally similar odorant molecules that share chemical features. This will lead to a systematic dependence of ensemble-level olfactory representations on odorant chemistry. To assess this dependence in *C. elegans*, we performed hierarchical clustering of the odorants in our stimulus panel based on the degree of similarity in the ensemble-level activities that they evoked at high concentrations (**Figure 2E**). We found that the representations of some molecular classes clustered together. For example, we found that ensemble-level responses to a set of straight-chain alcohols – 1-hexanol, 1-heptanol, 1-octanol, and 1-nonanol – were similar to one another. Likewise, the ensemble-level response to a set of ketones – 2-butanone, 2,3-pentanedione, and 2-heptanone – were similar to one another. The esters in our panel evoked a broader set of representations. We note that the esters we tested were structurally more diverse than either the alcohols or the ketones.

Principal component analysis (PCA) provides another way of assessing the similarity of ensemble-level representations to odorants. We constructed a principal component space from all measured ensemble-level representations, and asked how individual odorant responses are distributed in this space. Consistent with observations using hierarchical clustering, responses to certain classes of odorants, such as alcohols and ketones, are closer to each other in PCA space. Responses to members of other classes, such as esters, are distributed more broadly (**Figure 2F**).

PCA allows us to quantify the relative contribution of each sensory neuron to the total ensemble-level representation. We quantified the loading of the first three principal components by the activity of each sensory neuron (**Figure S3G**). We observed a broad distribution of principal component loading, which indicates that all eleven sensory neurons contribute to the animal's ability to discriminate odors, where we assume that ease of discrimination scales with the difference in ensemble-level representations.

Single trial responses suffice for odorant discrimination

Different odorants evoke different olfactory representations. Given trial-to-trial variability in single neuron responses, are olfactory representations sufficiently dissimilar for reliable odorant discrimination or identification based on single trials? To test this, we compiled all single-trial responses to each odorant across all datasets. In some recordings where data from individual neurons was missing, we imputed missing activity patterns using the rest of the ensemble (**Appendix D**, **Figure S5A-D**). In PCA space, chemically similar odorants have more similar representations (**Figure S5D**) and chemically dissimilar odorants have dissimilar representations (**Figure S5E**). However, overlap in a low-dimensional PCA space is a poor measure for odorant

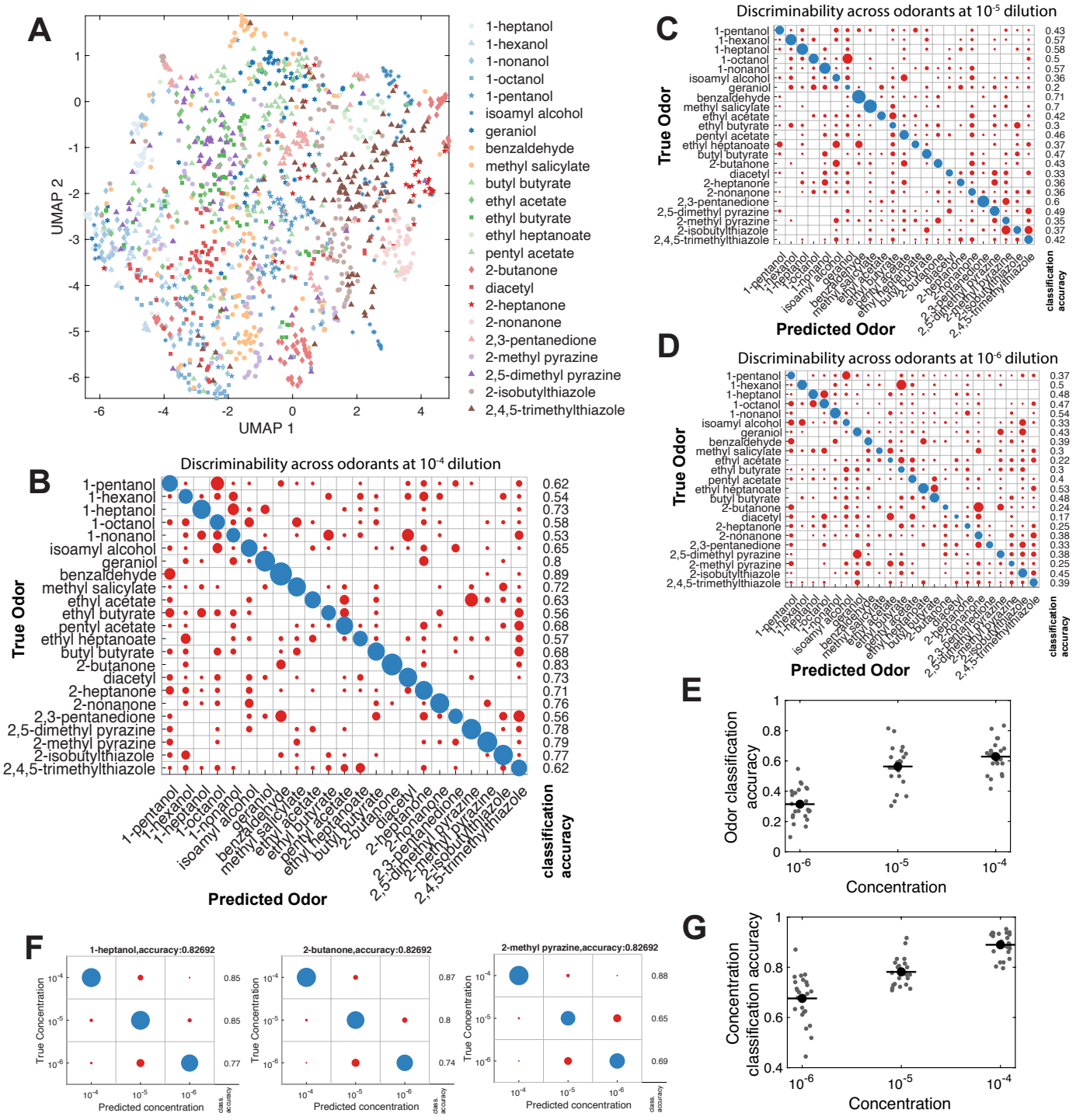

Figure 3. Representative comparisons of single-trial odorant responses. (A) A low-dimensional UMAP representation of single-trial neural responses to all 23 odorants at the 10^{-4} dilution. Responses to any given odorant generally cluster together. **(B)** Linear discriminability analysis of single-trial peak responses to high-concentration (10^{-4} dilution) odorants, with the presented odorant on the y-axis and the classified odorant on the x-axis. The size of each circle reflects the number of trials, with correct classifications colored blue and incorrect classifications colored red. To the right is printed the fraction of correctly classified trials for each odorant. We see that the majority of single trials are correctly classified by odorant delivered. At lower concentrations, 10^{-5} dilution **(C)** and 10^{-6} dilution **(D)**, odor classification accuracy diminishes. This is summarized in **(E)**, a scatterplot of the multi-class classification accuracy at different concentrations **(B, C, D)**. **(F)** Within a given odorant (three examples shown), the concentration of the odorant presented can be correctly classified based on the individual peak responses. **(G)** Across all odorants, concentration classification accuracy at different concentrations is shown in this scatterplot.

discrimination because <60% of the variance is explained by the first three principal components.

To better quantify and visualize ensemble-level responses to single odorant exposures, we performed dimensionality reduction of all single trial responses to all 23 odorants using Uniform Manifold Approximation and Projection (UMAP). In the UMAP space, single trial measurements of ensemble activities for the same odorant tended to cluster together, although activities for different odorants also tended to overlap (**Figure 3A**). To estimate discrimination based on single-trial measurements, we calculated errors in binary classification based on the pooled single-trial responses of each odorant pair using logistic regression (**Figure S5F**) and a Support Vector Machine (SVM) (**Figure S5G**). In all cases, binary classification succeeded with low error. Thus, single-trial ensemble-level responses of any two odorants are separable by linear classification.

Odorant identification based on single-trial responses

Next, we asked whether odorant identity could be uniquely decoded on the basis of single-trial ensemble-level responses, a task significantly more challenging than binary classification. To do this, we trained a multi-class classifier to perform linear discrimination. We randomly divided all single-trial measurements into a training set (90%) and validation set (10%). After we trained the classifier with the training set, we tested its performance in predicting odorant identities using single-trial measurements drawn from the validation set (see **Appendix E** for details). This classifier successfully identified odorants in the majority of single-trial measurements at high concentrations (**Figure 3B,E**). Classification accuracy declined at lower odorant concentrations, but succeeded in the plurality of measurements (**Figure 3C-E**).

We also asked whether odorant intensity could be estimated from single-trial measurements. To do this, we trained multi-class classifiers to predict the concentration of a given odorant using single-trial measurements. These classifiers were able to predict odorant concentration with high accuracy, although accuracy declined at lower concentrations (**Figure 3F-G**). We conclude that the ensemble-level spatial map of sensory neuron activity is sufficient to reliably determine odorant identity and intensity from single stimulus presentations.

Sensory neurons are broadly or narrowly tuned to olfactory stimuli

Olfactory sensory neurons are tuned to odorants by the relative binding affinities of their receptors for different ligands (57). In larger animals, the tuning of a given sensory neuron is defined by the chemical structure of the binding pocket of its associated olfactory receptor (4, 58–60). In *C. elegans*, the tuning of a sensory neuron is shaped by the expression of multiple olfactory receptors. We observed both broad and narrow tuning among different sensory neurons. For example, the AWA, AWB, AWC, and ASE sensory neurons are broadly tuned, each responding to most tested odorants at high concentrations (**Figure 2A-C, 4A**). In contrast, the ADF, ADL, ASG, ASI, ASJ, and ASK neurons are narrowly tuned, each responding to a small subset of odorants even at the highest tested concentrations. The ASH neuron is broadly tuned at high concentrations and narrowly tuned at low concentrations (**Figure 4A**), a pattern that might reflect its role as a nociceptor, mediating avoidance of any odorant when delivered at a sufficiently high concentration (**Figure 2**).

To visualize the tuning of each sensory neuron to odorants, we plotted significant neuronal responses ($q \leq 0.01$) in a space of chemical structure that we constructed using molecular descriptors of each odorant (**Figure S3A**). The responses of each sensory neuron occupy contiguous domains in the chemical structure space. These domains encompass chemically similar odorant molecules that are effective stimuli for each sensory neuron (**Figures 4B-E, S6**). At high concentrations, broadly tuned neurons such as AWA exhibit responses throughout the chemical structure space. Narrowly tuned neurons such as ADF extend responses over a smaller contiguous region of chemical space, even at high odorant concentrations.

At lower concentrations, most broadly tuned neurons extend their responses over a smaller region of chemical space, thereby revealing structural characteristics of the types of molecules to which each sensory neuron is most sensitive. AWA appears to be most strongly activated by ketones, AWB is most strongly activated by esters, and ASE is most activated by alcohols (**Figure S6**). At low concentrations, ASH responds to chemicals distributed throughout the chemical space, a breadth that may reflect the fact that any odorant delivered at sufficiently high concentration can evoke reflexive avoidance. The observation that each sensory neuron extends its sensitivity range across a contiguous region of chemical structural space suggests that each neuron is tuned to shared molecular properties of a set of odorant stimuli, as opposed to being faithful 'labeled-line' detectors of a set of unique odorants.

In larger animals, each sensory cell typically expresses single types of receptors. When domains of sensory neuron activity in larger animals are represented in a chemical structural space, such as the one that we used for *C. elegans*, response domains have been shown to be clustered. Their olfactory neuron ensembles are able to span the full range of chemical space by connecting the clustered response domains of different olfactory sensory neurons (1–6).

In *C. elegans*, the broad tuning of many sensory neurons is probably caused by the combined activities of many different olfactory receptors that are expressed in each neuron. Each receptor may be tuned to a smaller region of chemical structural space. Combining the regions of chemical structure space that are detected by each receptor produces the total region of space detected by the neuron. The tendency of even the most broadly tuned neurons to be principally activated by certain chemical classes suggests that the cell-specific expression of receptor molecules might be correlated. Each sensory neuron might express receptors that are individually most sensitive to chemically similar odorants, thereby broadening the tuning of the neuron to a larger set of similar odorant molecules when taken together.

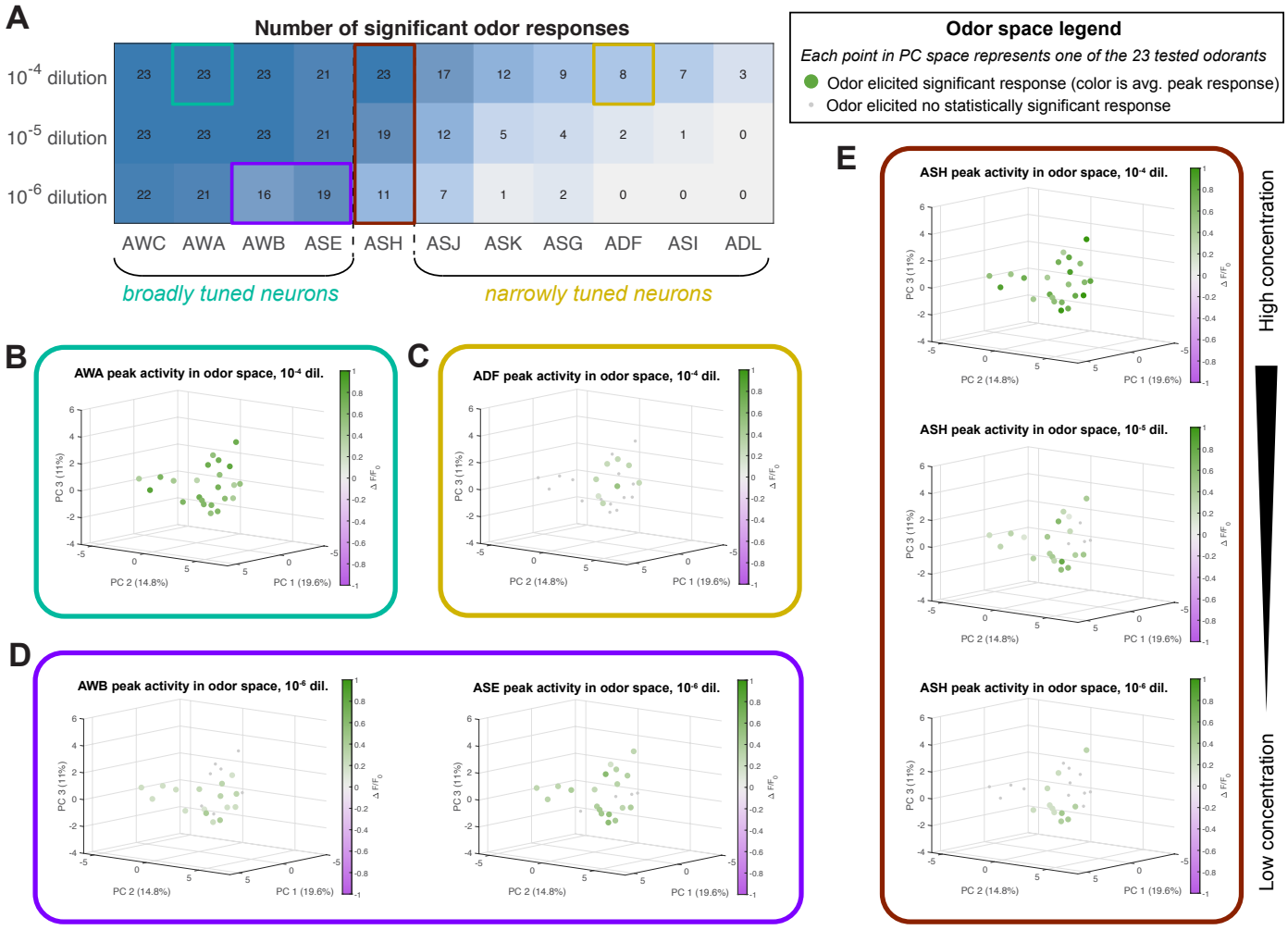

Figure 4. Chemosensory neuron tuning. (A) The number of odorants in our 23-odor panel which elicited significant responses ($q \leq 0.01$) in each neuron, at three different concentrations. We consider neurons which responded to the majority of presented odors as "broadly tuned", and neurons which responded to a small numbers of odors as "narrowly tuned". For each neuron, we plot the peak responses to the odors in an odor space constructed from chemical descriptors (**Figure S3A**). **(B)** The activity of broadly tuned neurons (ex: AWA) spans the odor space, while **(C)** the activity of narrowly tuned neurons (ex: ADF) is confined to a subset of chemically similar odorants. **(D)** At low concentrations, broadly tuned neurons respond to distinct subsets of odorants. **(E)** ASH, a polymodal nociceptor, is activated by all tested odorants at high concentration, but is only activated by a small set of repulsive odorants at low concentration. Refer to **Figure S6** for odor space plots for all neurons.

Sensory representations are not dependent on synaptic connections

All broadly and narrowly tuned sensory neurons synapse onto a set of interneurons – AIA, AIB, AIY, and AIZ – that participate in learned and innate olfactory behaviors (**Figure 1A**). These interneurons integrate olfactory information from the entire sensory periphery. Each sensory neuron, by virtue of its unique activity pattern across chemical space, provides different information to the interneurons that process olfactory stimuli into behavior. Broadly-tuned neurons may provide coarse-grained information about odorant identity, classifying broad families of odorant molecules. Narrowly-tuned neurons may provide fine-grained information about selected portions of chemical space. Taken together, the broadly and narrowly tuned neurons build a spatial map that may allow the identity and intensity of many odorants to be precisely and robustly decoded by the interneuron network for olfactory behavior.

The *C. elegans* connectome indicates that the chemosensory neurons are not simply feed-forward with respect to the interneurons for olfactory behavior. There are lateral connections between sensory neurons, such as ASI to AWC and AWB to ADF (25, 26). There are also feedback connections from interneurons to sensory neurons, such as AIA onto AWC. It has been suggested that feedback by neuropeptide signaling causes the ASE neuron to respond when benzaldehyde detected by other sensory neurons (37) We analyzed a synaptic communication mutant to assess the extent to which ensemble-level olfactory representations are shaped by communication between neurons.

We crossed our imaging line (ZM10104) with an *unc-13(s69)* synaptic transmission mutant (61). We presented these mutants with five odorants from our panel that represented multiple chemical groups. Nearly all the same neurons significantly responded ($q \leq 0.01$) in both wild-type and mutant animals (**Figure 5A**). Thus, synaptic communication does not appear to be a main driving force behind the spatial map that encodes odorant identity and intensity – similar neuronal ensembles respond to diverse olfactory stimuli in animals with or without chemical synaptic communication.

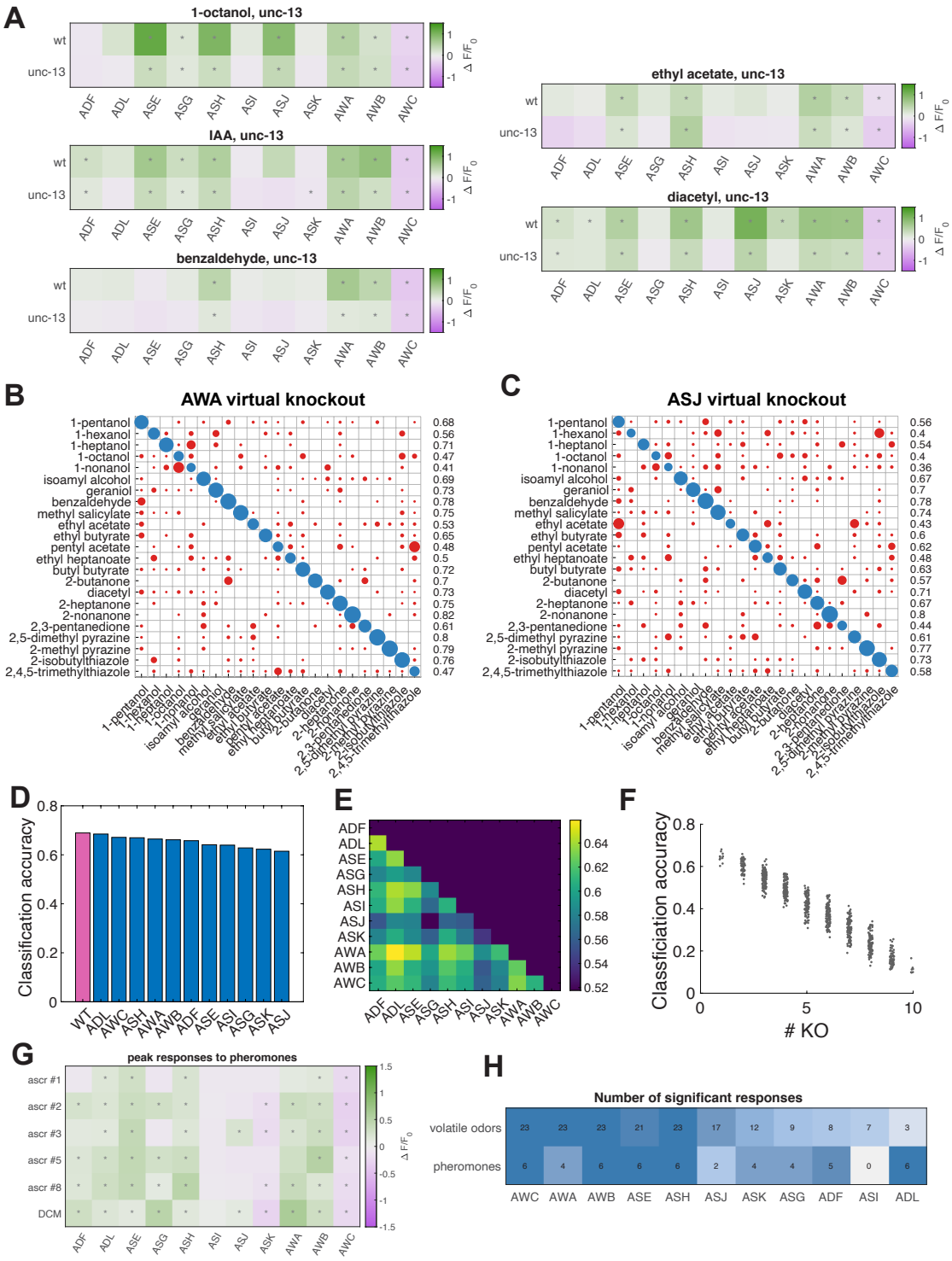

Figure 5. Impact of perturbations on odor representation. (A) We crossed the sensory neuron imaging line (ZM10104) with an *unc-13(s69)* synaptic transmission mutant, and recorded neural activity during odor presentation. We found that when presented with the same odorants, similar sets of neurons significantly ($q \leq 0.01$) responded in wild-type and *unc-13* mutant animals. Linear discriminability analysis of single-trial data, with **(B)** AWA or **(C)** ASJ virtually removed from the dataset. Removing different neurons changes the discriminability matrix in distinct ways. **(D)** We virtually removed each neuron from the dataset, and computed the average classification accuracy for each virtual knockout. We find that classification accuracy remains close to wild type (all 11 neurons), but is degraded more severely by the removal of narrowly tuned neurons (ASI, ASK, ASJ, ASG) than by the removal of broadly tuned neurons. **(E)** Virtually removing pairs of neurons, we see further reductions in average classification accuracy. **(F)** Plotting average classification accuracy of different sets of virtual knockouts, we observe a linear relationship between theoretical classification accuracy and the number of chemosensory neurons. **(G)** Average peak responses of the 11 chemosensory neurons to ascaroside pheromones #1, #2, #3, #5, and #8 at a concentration of 200 nM, and to dauer-conditioned media (DCM). Responses are reported as $\Delta F/F_0$, and significant responses ($q \leq 0.01$) are indicated with stars. **(H)** Comparing the fraction of volatile odorants (out of 23 odorants total) which elicited significant responses in each neuron at high concentration (first row) with the fraction of pheromone stimuli (out of 6 stimuli total) which elicited significant responses (second row).

Virtual neuron knockouts degrade classification accuracy

To quantify the relative contribution of each sensory neuron to ensemble-level discriminability, we performed virtual knockouts. We performed these virtual knockouts by removing (masking) specific sensory neurons from the dataset and retraining our multi-class classifier on the remaining data. Removing any single sensory neuron led to small decreases in classification accuracy compared to wild-type (**Figure 5B-D**). Classification accuracy was degraded more severely when narrowly tuned neurons such as ASI, ASK, ASJ, and ASG were masked than when broadly tuned neurons such as AWA, ASH, and AWC were masked.

The removal of different neurons degrades the classification accuracy of a given odorant to different degrees. For instance, pentyl acetate is correctly classified 68% of the time when all 11 chemosensory neurons are included in the dataset. ASJ masking reduces this accuracy to 62%, but AWA masking reduces accuracy to 48%.

Virtual masking of any two neurons further decreases average classification accuracy (**Figure 5E**). We also computed the average classification accuracy when randomly removing different combinations of multiple neurons. We observed an inverse linear relationship between the number of virtually masked neurons and classification accuracy (**Figure 5F**). Odor identity across olfactory space is thus encoded in a distributed manner across all 11 chemosensory neurons.

Pheromone representations are distinct from those of volatile odorants

Several sensory neurons (notably ADL, ADF, and ASK) play roles in the detection of ascaroside pheromones (62–67). We asked whether pheromone detection might also involve a distributed ensemble-level code like we observed for odorant detection. We presented young-adult hermaphrodites with a panel of five single ascarosides (#1, #2, #3, #5, and #8)(63) at a concentration of 200 nM. We also presented animals with dauer-conditioned media (DCM), supernatant from a population of animals grown in liquid culture that had starved and turned into dauers. DCM contains multiple pheromones, and is potentially a more naturalistic pheromone stimulus. We found that pheromones activated multiple chemosensory neuron classes (**Figure 5G**). Some neurons which were narrowly tuned to volatile odorants were strongly activated across the pheromone panel, including ADL, ADF, ASK, and ASG (**Figure 5H**). Pheromones also evoked some activity in the broadly tuned neurons, though AWA was activated less often by pheromones than by volatile odorants. Thus, the pheromone encoding appears to rely on many of the neurons that are narrowly tuned for volatile odorants.

Discussion

In insects and vertebrates, the integrated activity of large ensembles of chemosensory neurons is often presumed to enhance odorant discrimination and broaden the space of olfactory perceptions and behavioral responses. *C. elegans* uses an olfactory system with eleven pairs of distinct chemosensory neurons to navigate its environment, find food, avoid dangers, and detect other nematodes. Does *C. elegans* integrate information from multiple chemosensory neurons to help identify the many different olfactory cues that drive diverse behaviors? We have simultaneously recorded from all *C. elegans* chemosensory neurons in animals exposed to a large and chemically diverse odorant panel. These recordings have revealed that nearly every odorant stimulus evokes a distinct activity pattern in the chemosensory ensemble. Diverse and reproducible activity patterns encode odorant identity and intensity with precision and robustness.

Previous studies of the *C. elegans* olfactory system have largely dissected the properties of individual chemosensory neurons as they drive specific behaviors to selected odorants. For example, ASH has been characterized as a nociceptor that mediates reflexive avoidance to certain repellents (27–30). AWA, AWB, and AWC have well-characterized abilities to detect select odorants, mediating innate and learned navigational behaviors (27, 34, 36, 45, 68). Most previous studies have implicitly explored "labeled lines," where the activity patterns of single sensory neurons are directly mapped onto behavioral patterns. Indeed, single olfactory sensory neurons can exhibit complex temporal activity patterns in response to odorant stimulation. The complex activity patterns of single neurons such as AWA have been accurately and directly mapped to behavioral patterns (36, 37, 53, 68, 69). However, experiments where select odorants are used to stimulate sensory neurons do not explore how the animal encodes or discriminates between diverse olfactory inputs. Olfactory discrimination is necessary in an animal that performs a variety of behaviors in response to diverse olfactory cues in the natural world.

We have found that most olfactory stimuli activate multiple chemosensory neurons in *C. elegans* (**Figure 2**). We have shown that the chemosensory neurons that have been principally studied for roles in olfactory learning and navigation – AWA, AWB, AWC, and ASE – are also the neurons that are most broadly tuned to different chemicals. Each broadly tuned neuron may be more sensitive to a certain types of molecule. For instance, AWA is relatively strongly activated by ketones, while AWB is more strongly activated by some esters esters and ASE is more activated by alcohols. AWC is inhibited by every odorant that we studied. Other olfactory neurons – such as ASK, ASJ, or ASG – are more narrowly tuned, being activated by a small number of odorants in our stimulus panel with similar molecular features (**Figures 4, S6**).

When the activity patterns of all broadly and narrowly tuned chemosensory neurons are taken together, a reproducible and distinct spatial map of neuronal activity emerges for olfactory stimuli. This map encodes both odorant identity and intensity across the stimuli spanned by our panel of 23 diverse chemicals tested at multiple concentrations (**Figure 3**). Broadly tuned neurons allow coarse olfactory identification, while each narrowly tuned neuron is sensitive to a smaller region of olfactory space. When a narrowly tuned neuron is active, the possible identities of a new olfactory stimulus are circumscribed to those odorant molecules inside its range of neuronal sensitivity. When a narrowly tuned neuron is inactive, odorant molecules inside its sensitivity range are ruled out. When taken together, the patterns

of activity and inactivity of broadly and narrowly tuned neurons provide enough information to estimate the identity and concentration of any odorant with single stimulus presentations.

The extent to which any animal – *C. elegans*, insects, or vertebrates – exploits the collective activity of chemosensory neurons to decode odorant information is poorly understood. On one hand, the "dimensionality" of the olfactory code is often presumed to be as large as the number of distinct chemosensory neurons that contribute to the code (70). If so, the ability to detect even small numbers of different molecules, each with specificity to a different subsets of chemosensory neurons, can underlie the potential to discriminate astronomical numbers of olfactory stimuli (71). On the other hand, animals may trade a high-dimensional olfactory coding strategy for one that allows for rapid and efficient identification of odorants. This can be accomplished using a small number of the earliest responding (or primary) olfactory receptors and neurons, as seen in recent experiments with rodents that explore "primacy models" of the olfactory code(72).

Measuring the dimensionality of the neural code requires methods that record from large numbers of neurons at once. In *C. elegans*, large-scale multineuronal recording by volumetric imaging is a recent innovation (73, 74). The first brain-wide recordings of immobilized *C. elegans* – in animals exhibiting fictive forward and backward movements, either spontaneously or in response to a repellent (low oxygen levels) – revealed surprisingly few patterns of correlated global activity. One large group of neurons became active in the fictive forward state. Another large group of neurons became active in the fictive backward state. Both forward and backward states could be entrained to an attractive or repellent stimulus. However, low-dimensional brain-wide representation of behavioral state may also reflect the limited behavioral repertoire available to an immobilized animal (75, 76).

In another study of freely behaving males as they mated with hermaphrodites – a complex, multi-step, social behavior – a much greater diversity of brain-wide activity patterns was observed (77). Every distinguishable sensory pattern and motor sequence within the behavioral repertoire of a male *C. elegans* as he mated with a hermaphrodite could be associated with a unique pattern of brain-wide activity. The diversity of brain-wide activity patterns – made large by the combinatorial possibilities available to the small number of neurons in the male brain – matched the diversity of behavioral patterns. In this study, we simultaneously recorded from only eleven chemosensory neurons in *C. elegans*. The diversity of activity patterns available to the chemosensory ensemble allows one-to-one mapping to a much larger number of odorant stimuli than neurons.

Does *C. elegans* use all the information encoded in the combinatorial possibilities of its chemosensory ensemble to increase the variety of internal olfactory representations and outward behaviors? Answering this question requires high-dimensional measurements of olfactory perceptions and behaviors. One strategy is to make whole-brain recordings that extend from the chemosensory neurons that encode stimuli, to the interneurons that form perceptions, to the motor neurons that shape behavior. To this end, brain-wide approaches in *C. elegans* neuroscience are being developed. These include reagents for panneuronal cell identification, new genetic methods to label cells of interest with fluorescent reporters, and the assembly of reliable brain atlases for the *C. elegans* connectome (26, 41, 78, 79). Another strategy is to analyze behavior itself, and determine whether measurable differences in sensory representations can cause measurable differences in odorant-evoked behavior (74). Combining high-throughput odorant stimulation with brain-wide imaging and tracking in behaving animals is becoming possible with advances in microfluidics and imaging (48, 76, 80–82).

If the entire chemosensory ensemble is used to decode odorants, it is the unique response properties of each *C. elegans* chemosensory neuron that allows every neuron to contribute information to the overall spatial map that encodes olfactory stimuli. Removing any chemosensory neuron will lower the accuracy of stimulus classification based on ensemble activity (**Figure 5B-F**). Because the spatial map of chemosensory ensemble activity is largely independent of synaptic communication between neurons (**Figure 5A**), the tuning of each chemosensory neuron is, for the most part, a cell-intrinsic property. In *C. elegans*, the tuning of a given chemosensory neuron is shaped by the expression and properties of multiple receptors, not by the sensitivity of a single receptor as is typical in larger animals. We have uncovered a diversity of odorant dose-response curves in *C. elegans* (**Figure 2D, S3F**), which is also likely to be a direct result of the expression of multiple receptors. Variable dose-response curves may arise from the cumulative activities of many receptors with different binding affinities for a given odorant in each chemosensory neuron. Moreover, the sensitivity of both broadly and narrowly tuned chemosensory neurons reflects correlated sensitivities to similar odorant molecules (**Figures 4, S6**). Too little is known about the expression and properties of olfactory receptors in *C. elegans* to fully interpret the activity of any chemosensory cell in terms of receptor expression.

Comparing chemosensory ensemble responses to volatile odorants and pheromones, neurons that are narrowly tuned to volatile odorants are also those that are broadly tuned to pheromones and vice-versa (**Figure 5G-H**). We do not know if the activation of pheromone-sensing neurons by volatile odorants reflects cross-reactivity of pheromone receptors to small organic molecules, or whether these narrowly tuned neurons also express other olfactory receptors. Similarly, we do not know if the activation of broadly tuned olfactory neurons by pheromones reflects cross-reactivity of olfactory receptors to large organic pheromone molecules. In any case, widespread activity across all chemosensory neurons in response to either odorant and pheromone provides substantial information that can be used to identify any chemical stimulus.

We note that our analyses are coarse-grained measurements of the chemosensory neuron activity based on calcium imaging, and by looking primarily at peak responses, we omit differences in dynamics, spiking, or asymmetric responses, all of which likely encode additional information. Thus, our estimates of the information encoded in ensemble-level peak ac-

tivity of chemosensory neurons represent conservative lower bounds. How is the information contained in ensemble representations transformed into behavior? Downstream from the chemosensory ensemble, interneuron networks resemble both a reflexive avoidance circuit (consisting of the command interneurons AVA, AVB, and AVD that primarily receive inputs from ASH) and a circuit for learning and navigation (consisting of the interneurons AIA, AIB, AIY, and AIZ that integrate the activity of the entire chemosensory ensemble) (**Figure 1A**) (27–34). ASH might be part of a "nociceptive labeled line" that maps the detection of noxious stimuli to rapid escape responses, but the entire chemosensory ensemble also appears to be decoded by a more complex interneuron network.

Whether any animal uses ensemble representations to expand the dimensionality of olfactory space has been difficult to determine (70). This determination requires estimates of potentially astronomical numbers of distinct perceptions and verification that the animal projects these perceptions onto behavioral patterns in different ways. Here, we have shown that *C. elegans* may be an effective model for exploring the dimensionality of chemosensory representations and ensemble-level codes. The differences in the layout of the *C. elegans* olfactory system in comparison to insects and vertebrates notwithstanding, all of these animals exhibit widespread activities at their sensory peripheries to olfactory stimuli. There may be common principles by which all animals integrate the activity of distinct olfactory neurons to expand the range of olfactory perception. The small number of neurons in *C. elegans* can be interrogated at all levels from sensory input to interneurons to motor neurons. While the combinatorial possibilities of the olfactory code are still large in *C. elegans*, its relatively small size makes it a useful system to explore the possibility and relevance of ensemble-level codes in olfactory representation. Advances in brain-wide imaging, olfactory stimulus control, and behavior tracking will facilitate the quantitative mapping of large spaces of chemical stimuli to chemosensory ensemble activity to internal olfactory representations to behavioral patterns.

Methods

Worm maintenance

All *C. elegans* lines used in this project were grown at 22°C on nematode growth medium (NGM) plates seeded with the *E. coli* strain OP50. All animal lines were allowed to recover from starvation or freezing for at least two generations before being used in experiments. All animals used in experiments were young adults.

Plasmids and crosses

To construct the ZM10104 imaging strain we created and then crossed two integrated lines, one expressing GCaMP and one expressing the wCherry landmark. The first of these lines, ADS700, was made by co-injecting *lin-15(n765)* animals with pJH4039 (*ift-20* GCaMP6s::3xNLS) and a *lin-15* rescuing plasmid. A stable transgenic line (hpEx3942) with consistent GCaMP expression in the chemosensory neurons was selected for integration, and transgenic animals were irradiated with UV light to integrate the transgenes into the genome. The resulting integrated line (aeaIs008) was then backcrossed four times against N2 wild type. The second line, ADS701, was similarly made by co-injecting *lin-15(n765)* animals with pJH4040 (*gpc-1* wCherry) and a *lin-15* rescuing plasmid. A stable transgenic line with good wCherry expression was selected for integration, and transgenic animals were irradiated with UV light to integrate the transgenes into the genome. The resulting integrated line (hpIs728) was then backcrossed four times against N2 wild type. To make ZM10104, ADS700 hermaphrodites were crossed with N2 males. Heterozygous aeaIs008/+ male progeny were then crossed with ADS701 hermaphrodites. F1 progeny were picked for wCherry expression, and F2 progeny were picked for both GCaMP6s and wCherry expression. The line was then homozygosed in the F3 generation.

The ADS707 mutant imaging line was created by crossing the ZM10104 line with EG9631, an *unc-13(s69)* mutant obtained from the CGC (61). EG9631 hermaphrodites were crossed with ZM10104 males. Heterozygous (aeaIs008/+; hpIs728/+; +/*unc-13*) F1 hermaphrodite progeny were selected by GCaMP6s and wCherry expression and wild type locomotion (*unc-13* is recessive). F2 progeny were picked for fluorescence and the *unc-13* uncoordinated phenotype. The line was then homozygosed for fluorescence in the F3 generation.

Microfluidics

We used a modified version of a microfluidic system capable of delivering multiple odors to *Drosophila* larvae (4). The microfluidics chip is designed with an arbor containing delivery points for multiple stimuli, together with a buffer delivery point and two control switches, one for buffer and one for odor (**Figure 1B**).

At any given time, three flows are active: one of the control switches, the buffer blank, and one odor stimulus. The chip is designed to maintain laminar flow of each fluid, and the flow is split between a waste channel and an odor channel which flows past the animal's nose. The chip described here is designed to switch rapidly from one stimulus to the buffer. After the flows pass the animal, they exit the chip via a waste port at atmospheric pressure. Waste is then removed with a vacuum.

We grafted the odorant delivery arbor to a *C. elegans* loading chamber similar to those designed by Chronis, et al. (48). We designed a loading chamber suitable for adult *C. elegans*, a narrow channel 62 µm wide and 30 µm high, with a gently tapered end. The tapered end serves as a guide to help hold the animal's nose in place without distorting the animal.

The microfluidic device pattern was designed in AutoCAD, and the design was translated to silicon wafer using photolithography. The photomasks of the design were printed using CAD/Art Services, Inc. The silicon wafer was then used as a mold for polydimethylsiloxane (PDMS) to fabricate microfluidic devices. The PDMS components were then removed from the silicon wafer, cut to size, and had access channels made with a biopsy punch. The completed PDMS components were then plasma bonded to No. 1 glass cover slips. To minimize contamination from dust, all microfluidics assembly was done in a cleanroom.

Preparation of odorant and buffer solutions

Odorants were diluted in CTX buffer (5 mM KH_2PO_4/K_2HPO_4 at pH 6, 1 mM $CaCl_2$, 1 mM $MgSO_4$, 50 mM NaCl, adjusted to 350 mOsm/L with sorbitol). To prevent contamination, each odor condition was mixed and stored in its own glass bottle, and delivered through its own glass syringe and tubing. Furthermore, a new microfluidic device was used for a single consistent panel of odors.

The single ascarosides (63) were diluted in CTX buffer to a concentration of 200 mM for presentation to the animals. Dauer-conditioned media (DCM) was prepared in a similar method to Butcher et al.(83). Animals grown on NGM plates were starved, so that most of the population was larvae. The animals were then rinsed off the plates using M9 buffer and transferred to 150 mL of S-complete in a 500 mL Erlenmeyer flask under sterile conditions. 150 µL of concentrated E. coli OP50 (80mg/mL) was added to the flask as a food source. The flask was then grown at room temperature on a shaker at 120 rpm for 4 weeks. From week 1 to week 3, 300 µL of OP50 was added to the flask on a weekly basis using sterile techniques. After the last feeding on the third week, the animals were let to starve and turn into dauers. The culture was harvested no later than 2 weeks after the last feeding. The liquid culture was collected and then centrifuged to isolate the supernatant (the DCM). The The DCM was then filtered through a 0.2 µm vacuum filter Sarstedt Inc. to remove any remaining bacteria and animals. It was flash frozen in a dry ice/ethanol bath and then stored at -80 °C.

Imaging setup

We employed a single-photon, spinning-disk confocal microscope to capture fluorescent images from intact *C. elegans*. The microscope was inverted to allow for easy access to the microfluidics device mounted on the stage. We employed a 488 nm laser to excite GCaMP *in vivo*, and used a 561 nm laser to excite the wCherry landmark. To minimize crosstalk between channels, lasers were fired sequentially during multicolor recordings. We captured images with a 60x water-immersion objective with an NA of 1.2. Volumes were acquired using unidirectional scans of a piezo objective scanner. All fluorescence microscopy is a trade-off between spatial resolution, temporal resolution, laser power, and signal strength. We optimized two sets of imaging conditions, one set for activity imaging and another set for landmark imaging. Both sets of imaging conditions capture the region containing the majority of the neurons in the head of *C. elegans*, a volume of 112 µm by 56 µm by 30 µm.

In any given experiment, acquisition of a landmark volume precedes acquisition of an activity movie. This volume, which contains both green and red channels, allows us to identify neurons of interest. The spatial resolution of these volumes is 0.5 µm x 0.5 µm x 1.5 µm/voxel, with the z-resolution of 1.5 µm set by the point spread function.

The activity movies were acquired at a high speed in the green channel only, with lower spatial resolution (1 µm x 1 µm x 1.5 µm/voxel). At this resolution, we could acquire volumes at a rate of 2.5 Hz in standard acquisition mode.

Analyzing multi-neuronal recordings

The neurons in each activity recording were identified and then tracked through time using a neighborhood correlation tracking method. The criteria for identifying each neuron class are described in Appendix A. Neurons which could not be unambiguiously identified were excluded from the dataset. All neuron tracks were then manually proofread to exclude mis-tracked neurons. Activity traces were bleach corrected and reported in:

$$\frac{\Delta F}{F_0} = \frac{F(t) - F_0}{F_0}. \tag{1}$$

Normalization by baseline fluorescence F_0 allowed for direct comparisons within a given neuron class across L/R and across individuals. The baseline F_0 value was determined individually for every recorded neuron, set at the 5th percentile of the distribution of bleach-corrected fluorescence values, with the opportunity for manual correction.

We employed 2-tailed, paired t-tests to compare the mean signal during stimulus presentation with an unstimulated period of identical length within the same neuron. Neurons were tested for both ON and OFF responses. The p-values were corrected for multiple testing using FDR (84). To test for asymmetric neuron responses, we used 2-tailed, two-sample t-tests (unpaired).

AUTHOR CONTRIBUTIONS

A.L., S.Q., H.C., V.V., M.Z. and A.S contributed to writing this manuscript. A.L., V.V., and A.S. designed the experiments. A.L., M.W., W.H., and M.Z. designed and built the transgenic *C. elegans* strains used in this project. A.L. and V.V. designed and built the imaging setup, microfluidics devices, and the wrote the software to extract neural traces. A.L., H.C., G.C., N.T., and R.V. carried out the imaging experiments and analyzed the data. A.L., S.Q., and C.P. developed the theoretical models. L.L. prepared the DCM reagent.

ACKNOWLEDGEMENTS We thank Guangwei Si and Jessleen Kanwal for their advice on microfluidics design and operation and Maedeh Seyedolmohadesin and Mahdi Torkashvand for our discussions on ascaroside responses. We also thank Sandeep Robert Datta, Steven Flavell, and the members of the Zhen, Pehlevan, and Samuel labs for their advice on the project and comments on the manuscript. The EG9631 strain was obtained from the CGC, which is funded by the NIH Office of Research Infrastructure Programs (P40 OD010440). Microfluidics devices were manufactured using the Soft Materials Cleanroom facility of the Harvard MRSEC (DMR-1420570). This work was supported by the NSF Brain Eager (NSF IOS-1452593), NSF Physics of the Living System (NSF 1806818), and NSF Ideas (NSF IOS-1555914) grants.

References

1. B Malnic, J Hirono, T Sato, and L B Buck. Combinatorial receptor codes for odors. *Cell*, 96(5): 713–23, 1999. ISSN 0092-8674. doi: 10.1016/S0092-8674(00)80581-4.
2. Kiyomitsu Nara, Luis R. Saraiva, Xiaolan Ye, and Linda B. Buck. A large-scale analysis of odor coding in the olfactory epithelium. *J. Neurosci.*, 31(25):9179–9191, 2011. ISSN 02706474. doi: 10.1523/JNEUROSCI.1282-11.2011.
3. Scott A. Kreher, Dennis Mathew, Junhyong Kim, and John R. Carlson. Translation of Sensory Input into Behavioral Output via an Olfactory System. *Neuron*, 59(1):110–124, 2008. ISSN 08966273. doi: 10.1016/j.neuron.2008.06.010.
4. Guangwei Si, Jessleen K. Kanwal, Yu Hu, Christopher J. Tabone, Jacob Baron, Matthew Berck, Gaetan Vignoud, and Aravinthan D.T. Samuel. Structured Odorant Response Patterns across a Complete Olfactory Receptor Neuron Population. *Neuron*, 101(5):950–962.e7, mar 2019. ISSN 10974199. doi: 10.1016/j.neuron.2018.12.030.
5. Jing W. Wang, Allan M. Wong, Jorge Flores, Leslie B. Vosshall, and Richard Axel. Two-photon calcium imaging reveals an odor-evoked map of activity in the fly brain. *Cell*, 112(2):271–282, 2003. ISSN 00928674. doi: 10.1016/S0092-8674(03)00004-7.
6. Elissa A. Hallem and John R. Carlson. Coding of Odors by a Receptor Repertoire. *Cell*, 125(1): 143–160, 2006. ISSN 00928674. doi: 10.1016/j.cell.2006.01.050.
7. Josefina del Marmol, Mackenzie A Yedlin, and Vanessa Ruta. The structural basis of odorant recognition in insect olfactory receptors. *Nature (London)*, 597(7874):126–131, 2021. ISSN 0028-0836.
8. M. De Bruyne and T. C. Baker. Odor detection in insects: Volatile codes. *J. Chem. Ecol.*, 34(7): 882–897, 2008. ISSN 00980331. doi: 10.1007/s10886-008-9485-4.
9. Leslie B. Vosshall and Reinhard F. Stocker. Molecular architecture of smell and taste in Drosophila. *Annu. Rev. Neurosci.*, 30:505–533, 2007. ISSN 0147006X. doi: 10.1146/annurev.neuro.30.051606.094306.

10. Chih Ying Su, Karen Menuz, and John R. Carlson. Olfactory Perception: Receptors, Cells, and Circuits. *Cell*, 139(1):45–59, 2009. ISSN 00928674. doi: 10.1016/j.cell.2009.09.015.
11. John G. Hildebrand and Gordon M. Shepherd. Mechanisms of olfactory discrimination: Converging evidence for common principles across phyla. *Annu. Rev. Neurosci.*, 20:595–631, 1997. ISSN 0147006X. doi: 10.1146/annurev.neuro.20.1.595.
12. Barry W. Ache and Janet M. Young. Olfaction: Diverse species, conserved principles. *Neuron*, 48(3):417–430, 2005. ISSN 08966273. doi: 10.1016/j.neuron.2005.10.022.
13. Leslie M. Kay and Mark Stopfer. Information processing in the olfactory systems of insects and vertebrates. *Semin. Cell Dev. Biol.*, 17(4):433–442, 2006. ISSN 10849521. doi: 10.1016/j.semcdb.2006.04.012.
14. Ariane Ramaekers, Edwige Magnenat, Elizabeth C. Marin, Nanaë Gendre, Gregory S.X.E. Jefferis, Liqun Luo, and Reinhard F. Stocker. Glomerular maps without cellular redundancy at successive levels of the Drosophila larval olfactory circuit. *Curr. Biol.*, 15(11):982–992, 2005. ISSN 09609822. doi: 10.1016/j.cub.2005.04.032.
15. R. F. Stocker, M. C. Lienhard, A. Borst, and K. F. Fischbach. Neuronal architecture of the antennal lobe in Drosophila melanogaster. *Cell Tissue Res.*, 262(1):9–34, 1990. ISSN 0302766X. doi: 10.1007/BF00327741.
16. Dara L. Sosulski, Maria Lissitsyna Bloom, Tyler Cutforth, Richard Axel, and Sandeep Robert Datta. Distinct representations of olfactory information in different cortical centres. *Nature*, 472 (7342):213–219, 2011. ISSN 00280836. doi: 10.1038/nature09868.
17. Sepideh Keshavarzi, John M. Power, Eva H.H. Albers, Robert K.S. Sullivan, and Pankaj Sah. Dendritic organization of olfactory inputs to medial amygdala neurons. *J. Neurosci.*, 35(38): 13020–13028, 2015. ISSN 15292401. doi: 10.1523/JNEUROSCI.0627-15.2015.
18. Kevin A. Bolding and Kevin M. Franks. Recurrent cortical circuits implement concentration-invariant odor coding. *Science (80-.).*, 361(6407), 2018. ISSN 10959203. doi: 10.1126/science.aat6904.
19. P.S. Grewal and D.J. Wright. Migration of Caenorhabditis elegans larvae towards bacteria and the nature of the bacterial stimulus. *Fundam. Appl. Nematol.*, 15:159–166, 1992.
20. Cornelia I Bargmann. Comparative chemosensation from receptors to ecology. *Nature (London)*, 444(7117):295–301, 2006. ISSN 0028-0836.
21. Cornelia I. Bargmann. Chemosensation in *C. elegans*. *WormBook : the online review of C. elegans biology*, pages 1–29, 2006. ISSN 15518507. doi: doi:10.1895/wormbook.1.123.1.
22. Berta Vidal, Ulkar Aghayeva, Haosheng Sun, Chen Wang, Lori Glenwinkel, Emily A. Bayer, and Oliver Hobert. An atlas of Caenorhabditis elegans chemoreceptor expression. *PLoS Biol.*, 16: 1–34, 2018.
23. LA Perkins, EM Hedgecock, JN Thomson, and JG Culotti. Mutant sensory cilia in the nematode C. elegans. *Dev. Biol.*, 117:456–487, 1986.
24. Athanasios Metaxakis, Dionysia Petratou, and Nektarios Tavernarakis. Multimodal sensory processing in Caenorhabditis elegans. *Open Biol.*, 8(6), 2018. ISSN 20462441. doi: 10.1098/rsob.180049.
25. John G White, E Southgate, J N Thomson, and Sydney Brenner. The structure of the nervous system of the nematode Caenorhabditis elegans. *Philosophical Transactions of the Royal Society of London B*, 314:1–340, 1986.
26. Daniel Witvliet, Ben Mulcahy, James K Mitchell, Yaron Meirovitch, Daniel K Berger, Yuelong Wu, Yufang Liu, Wan Xian Koh, Rajeev Parvathala, Douglas Holmyard, et al. Connectomes across development reveal principles of brain maturation in C. elegans. *bioRxiv*, 2020.
27. Cornelia I Bargmann and H Robert Horvitz. Chemosensory Neurons with Overlapping Functions Direct Chemotaxis to Multiple Chemicals in C. elegans. *Neuron*, 7:729–742, 1991.
28. Massimo A. Hilliard, Cornelia I. Bargmann, and Paolo Bazzicalupo. C. elegans responds to chemical repellents by integrating sensory inputs from the head and the tail. *Current Biology*, 12(9):730–734, 2002.
29. Massimo A. Hilliard, Carmela Bergamasco, Salvatore Arbucci, Ronald H.A. Plasterk, and Paolo Bazzicalupo. Worms taste bitter: ASH neurons, QUI-1, GPA-3 and ODR-3 mediate quinine avoidance in Caenorhabditis elegans. *EMBO J.*, 23(5):1101–1111, 2004. ISSN 02614189. doi: 10.1038/sj.emboj.7600107.
30. Yoshihiro Sambongi, Takashi Nagae, Yanna Liu, Takao Yoshimizu, Kenji Takeda, Yoh Wada, and Masamitsu Futai. Sensing of cadmium and copper ions by externally exposed ADL, ASE, and ASH neurons elicits avoidance response in Caenorhabditis elegans. *Neuroreport*, 10(4): 753–757, 1999. ISSN 09594965. doi: 10.1097/00001756-199903170-00017.
31. Tokumitsu Wakabayashi, Izumi Kitagawa, and Ryuzo Shingai. Neurons regulating the duration of forward locomotion in Caenorhabditis elegans. *Neurosci. Res.*, 50(1):103–111, 2004. ISSN 01680102. doi: 10.1016/j.neures.2004.06.005.
32. Sreekanth H Chalasani, Nikos Chronis, Makoto Tsunozaki, Jesse M Gray, Daniel Ramot, Miriam B Goodman, and Cornelia I Bargmann. Dissecting a circuit for olfactory behaviour in Caenorhabditis elegans Gene-specific control of inflammation by TLR-induced chromatin modifications. *Nature*, 451(January):6540–6540, nov 2008. doi: 10.1038/nature06540.
33. Paul A. Garrity, Miriam B. Goodman, Aravinthan D. Samuel, and Piali Sengupta. Running hot and cold: Behavioral strategies, neural circuits, and the molecular machinery for thermotaxis in C. elegans and Drosophila. *Genes Dev.*, 24(21):2365–2382, 2010. ISSN 08909369. doi: 10.1101/gad.1953710.
34. Heon ick Ha, Michael Hendricks, Yu Shen, Christopher V. Gabel, Christopher Fang-Yen, Yuqi Qin, Daniel Colón-Ramos, Kang Shen, Aravinthan D.T. Samuel, and Yun Zhang. Functional Organization of a Neural Network for Aversive Olfactory Learning in Caenorhabditis elegans. *Neuron*, 68(6):1173–1186, 2010. ISSN 08966273. doi: 10.1016/j.neuron.2010.11.025.
35. Kazushi Yoshida, Takaaki Hirotsu, Takanobu Tagawa, Shigekazu Oda, Tokumitsu Wakabayashi, Yuichi Iino, and Takeshi Ishihara. Odour concentration-dependent olfactory preference change in C. elegans. *Nat. Commun.*, 3, 2012. ISSN 20411723. doi: 10.1038/ncomms1750.
36. Johannes Larsch, Donovan Ventimiglia, Cornelia I. Bargmann, and Dirk R. Albrecht. High-throughput imaging of neuronal activity in Caenorhabditis elegans. *Proceedings of the National Academy of Sciences of the United States of America*, 110(45), nov 2013. ISSN 00278424. doi: 10.1073/pnas.1318325110.
37. Sarah G. Leinwand, Claire J. Yang, Daphne Bazopoulou, Nikos Chronis, Jagan Srinivasan, and Sreekanth H. Chalasani. Circuit mechanisms encoding odors and driving aging-associated behavioral declines in Caenorhabditis elegans. *Elife*, 4(September 2015):1–26, 2015. ISSN 2050084X. doi: 10.7554/eLife.10181.
38. Alon Zaslaver, Idan Liani, Oshrat Shtangel, Shira Ginzburg, Lisa Yee, and Paul W Sternberg. Hierarchical sparse coding in the sensory system of Caenorhabditis elegans. *Proc. Natl. Acad. Sci. U. S. A.*, 112(4):1185–9, 2015. ISSN 1091-6490. doi: 10.1073/pnas.1423656112.
39. Sidney Yu, Leon Avery, Eric Baude, and David L. Garbers. Guanylyl cyclase expression in specific sensory neurons: A new family of chemosensory receptors. *Proc. Natl. Acad. Sci. U. S. A.*, 94(7):3384–3387, 1997. ISSN 00278424. doi: 10.1073/pnas.94.7.3384.
40. P. D. Wes and C. I. Bargmann. C. elegans odour discrimination requires asymmetric diversity in olfactory neurons. *Nature*, 410(6829):698–701, 2001. ISSN 00280836. doi: 10.1038/35070581.
41. Eviatar Yemini, Albert Lin, Amin Nejatbakhsh, Erdem Varol, Ruoxi Sun, Gonzalo E. Mena, Aravinthan D.T. Samuel, Liam Paninski, Vivek Venkatachalam, and Oliver Hobert. NeuroPAL: A Multicolor Atlas for Whole-Brain Neuronal Identification in C. elegans. *Cell*, 184:272–288, 2021. doi: 10.1016/j.cell.2020.12.012.
42. Makoto Tsunozaki, Sreekanth H Chalasani, and Cornelia I Bargmann. A behavioral switch: cgmp and pkc signaling in olfactory neurons reverses odor preference in c. elegans. *Neuron (Cambridge, Mass.)*, 59(6):959–971, 2008. ISSN 0896-6273.
43. Tod R. Thiele, Serge Faumont, and Shawn R. Lockery. Articles, Behavioral/Systems/Cognitive The Neural Network for Chemotaxis to Tastants in Caenorhabditis elegans Is Specialized for Temporal Differentiation. *Journal of Neuroscience*, 23:11904–11911, 2005.
44. Hiroshi Suzuki, Tod R. Thiele, Serge Faumont, Marina Ezcurra, Shawn R. Lockery, and William R. Schafer. Functional asymmetry in Caenorhabditis elegans taste neurons and its computational role in chemotaxis. *Nature*, 454(7200):114–117, jul 2008. ISSN 14764687. doi: 10.1038/nature06927.
45. Cornelia I Bargmann, Erika Hartwieg, and H Robert Horvitz. Odorant-Selective Genes and Neurons Mediate Olfaction in C. elegans. *Neuron*, 74:515–527, 1993.
46. Soleil E. Worthy, Lillian Haynes, Melissa Chambers, Danika Bethune, Emily Kan, Kevin Chung, Ryan Ota, Charles J. Taylor, and Elizabeth E. Glater. Identification of attractive odorants released by preferred bacterial food found in the natural habitats of C. elegans. *PLoS One*, 13(7): 1–14, 2018. ISSN 19326203. doi: 10.1371/journal.pone.0201158.
47. Guangshuo Ou, Makato Koga, Oliver E Blacque, Takashi Murayama, Yasumi Ohshima, Jenny C Schafer, Chunmei Li, Bradley K Yoder, Michel R Leroux, and Jonathan M Scholey. Sensory ciliogenesis in caenorhabditis elegans: Assignment of ift components into distinct modules based on transport and phenotypic profiles. *Molecular biology of the cell*, 18(5):1554–1569, 2007. ISSN 1059-1524.
48. Nikos Chronis, Manuel Zimmer, and Cornelia I. Bargmann. Microfluidics for in vivo imaging of neuronal and behavioral activity in Caenorhabditis elegans. *Nature Methods*, 4(9):727–731, sep 2007. ISSN 15487091. doi: 10.1038/nmeth1075.
49. Rafi Haddad, Rehan Khan, Yuji K. Takahashi, Kensaku Mori, David Harel, and Noam Sobel. A metric for odorant comparison. *Nat. Methods*, 5(5):425–429, 2008. ISSN 15487091. doi: 10.1038/nmeth.1197.
50. P. Sengupta, J. H. Chou, and C. I. Bargmann. odr-10 Encodes a seven transmembrane domain olfactory receptor required for responses to the odorant diacetyl. *Cell*, 84(6):899–909, 1996. ISSN 00928674. doi: 10.1016/S0092-8674(00)81068-5.
51. H. Sass. Sensory encoding of odor stimuli in Periplaneta americana. *J. Comp. Physiol. A Neuroethol. Sens. Neural Behav. Physiol.*, 107:49–65, 1976.
52. Markus Meister and Tobias Bonhoeffer. Tuning and Topography in an Odor Map on the Rat Olfactory Bulb. *J. Neurosci.*, 21(4):1351–1360, feb 2001. ISSN 0270-6474. doi: 10.1523/JNEUROSCI.21-04-01351.2001.
53. Emily R. Troemel, Bruce E. Kimmel, and Cornelia I. Bargmann. Reprogramming chemotaxis responses: Sensory neurons define olfactory preferences in C. elegans. *Cell*, 91(2):161–169, 1997. ISSN 00928674. doi: 10.1016/S0092-8674(00)80399-2.
54. Kentaro Kajiya, Koichiro Inaki, Motonari Tanaka, Tatsuya Haga, Hiroshi Kataoka, and Kazushige Touhara. Molecular bases of odor discrimination: Reconstitution of olfactory receptors that recognize overlapping sets of odorants. *J. Neurosci.*, 21(16):6018–6025, 2001. ISSN 02706474. doi: 10.1523/jneurosci.21-16-06018.2001.
55. Hartwig Spors, Matt Wachowiak, Lawrence B. Cohen, and Rainer W. Friedrich. Temporal dynamics and latency patterns of receptor neuron input to the olfactory bulb. *J. Neurosci.*, 26(4): 1247–1259, 2006. ISSN 02706474. doi: 10.1523/JNEUROSCI.3100-05.2006.
56. Martin Chalfie, John E. Sulston, John G. White, Eileen Southgate, J. Nichol Thomson, and Sydney Brenner. The neural circuit for touch sensitivity in Caenorhabditis elegans. *J. Neurosci.*, 5(4):956–964, 1985. ISSN 02706474. doi: 10.1523/jneurosci.05-04-00956.1985.
57. Josefina del Mármol, Mackenzie A. Yedlin, and Vanessa Ruta. The structural basis of odorant recognition in insect olfactory receptors. *Nature*, 597(7874):126–131, 2021. ISSN 14764687. doi: 10.1038/s41586-021-03794-8.
58. Harumi Saito, Qiuyi Chi, Hanyi Zhuang, Hiroaki Matsunami, and Joel D Mainland. Odor coding by a mammalian receptor repertoire. *Science signaling*, 2(60):ra9–ra9, 2009.
59. David Zwicker, Arvind Murugan, and Michael P. Brenner. Receptor arrays optimized for natural odor statistics. *Proc. Natl. Acad. Sci. U. S. A.*, 113(20):5570–5575, 2016. ISSN 10916490. doi: 10.1073/pnas.1600357113.
60. Shanshan Qin, Qianyi Li, Chao Tang, and Yuhai Tu. Optimal compressed sensing strategies for an array of nonlinear olfactory receptor neurons with and without spontaneous activity. *Proc. Natl. Acad. Sci. U. S. A.*, 116(41):20286–20295, 2019. ISSN 10916490. doi: 10.1073/pnas.1906571116.
61. AM Rose and DL Baillie. Genetic organization of the region around unc-15 (i), a gene affecting paramyosin in caenorhabditis elegans. *Genetics*, 96(3):639–48, 1980.
62. Evan Z. MacOsko, Navin Pokala, Evan H. Feinberg, Sreekanth H. Chalasani, Rebecca A. Butcher, Jon Clardy, and Cornelia I. Bargmann. A hub-and-spoke circuit drives pheromone attraction and social behaviour in C. elegans. *Nature*, 458(7242):1171–1175, 2009. ISSN 00280836. doi: 10.1038/nature07886.
63. Anusha Narayan, Vivek Venkatachalam, Omer Durak, Douglas K. Reilly, Neelanjan Bose, Frank C. Schroeder, Aravinthan D.T. Samuel, Jagan Srinivasan, and Paul W. Sternberg. Contrasting responses within a single neuron class enable sex-specific attraction in Caenorhabditis elegans. *Proc. Natl. Acad. Sci. U. S. A.*, 113(10):E1392–E1401, 2016. ISSN 10916490. doi: 10.1073/pnas.1600786113.
64. Joshua S Greene, Maximillian Brown, May Dobosiewicz, Itzel G Ishida, Evan Z Macosko, Xinxing Zhang, Rebecca A Butcher, Devin J Cline, Patrick T. McGrath, and Cornelia I Bargmann. Balancing selection shapes density-dependent foraging behaviour. *Nature*, 539(7628):254–258, 2016. ISSN 14764687. doi: 10.1038/nature19848.

65. Erin Z. Aprison and Ilya Ruvinsky. Counteracting Ascarosides Act through Distinct Neurons to Determine the Sexual Identity of C. elegans Pheromones. *Curr. Biol.*, 27(17):2589–2599.e3, 2017. ISSN 09609822. doi: 10.1016/j.cub.2017.07.034.
66. Kelli A. Fagan, Jintao Luo, Ross C. Lagoy, Frank C. Schroeder, Dirk R. Albrecht, and Douglas S. Portman. A Single-Neuron Chemosensory Switch Determines the Valence of a Sexually Dimorphic Sensory Behavior. *Curr. Biol.*, 28(6):902–914.e5, 2018. ISSN 09609822. doi: 10.1016/j.cub.2018.02.029.
67. Patrick T. McGrath and Ilya Ruvinsky. A primer on pheromone signaling in Caenorhabditis elegans for systems biologists. *Current Opinion in Systems Biology*, pages 23–30, 2019. doi: https://doi.org/10.1016/j.coisb.2018.08.012.
68. Ian G McLachlan, Talya S Kramer, Malvika Dua, Elizabeth M Diloreto, Ugur Dag, Jagan Srinivasan, and Steven W. Flavell. Diverse states and stimuli tune olfactory receptor expression levels to modulate food-seeking behavior. *bioRxiv*, pages 1–47, 2022.
69. Qiang Liu, Philip B. Kidd, May Dobosiewicz, and Cornelia I. Bargmann. C. elegans AWA Olfactory Neurons Fire Calcium-Mediated All-or-None Action Potentials. *Cell*, 175(1):57–70.e17, sep 2018. ISSN 10974172. doi: 10.1016/j.cell.2018.08.018.
70. Markus Meister. On the dimensionality of odor space. *Elife*, 4(JULY 2015):1–12, 2015. ISSN 2050084X. doi: 10.7554/eLife.07865.
71. C. Bushdid, M. O. Magnasco, L. B. Vosshall, and A. Keller. Humans Can Discriminate More than 1 Trillion Olfactory Stimuli. *Science (80-.).*, 343(6177):1370–1372, mar 2014. ISSN 0036-8075. doi: 10.1126/science.1249168.
72. Christopher D. Wilson, Gabriela O. Serrano, Alexei A. Koulakov, and Dmitry Rinberg. A primacy code for odor identity. *Nat. Commun.*, 8(1), 2017. ISSN 20411723. doi: 10.1038/s41467-017-01432-4.
73. Harris S. Kaplan and Manuel Zimmer. Brain-wide representations of ongoing behavior: a universal principle? *Current Opinion in Neurobiology*, 64:60–69, 2020. ISSN 18736882. doi: 10.1016/j.conb.2020.02.008.
74. Albert Lin, Daniel Witvliet, Luis Hernandez-Nunez, Scott W. Linderman, Aravinthan D. T. Samuel, and Vivek Venkatachalam. Imaging whole-brain activity to understand behaviour. *Nature Reviews Physics*, 0123456789, 2022. doi: 10.1038/s42254-022-00430-w.
75. Saul Kato, Harris S. Kaplan, Tina Schrödel, Susanne Skora, Theodore H. Lindsay, Eviatar Yemini, Shawn Lockery, and Manuel Zimmer. Global Brain Dynamics Embed the Motor Command Sequence of Caenorhabditis elegans. *Cell*, 163(3):656–669, oct 2015. ISSN 10974172. doi: 10.1016/j.cell.2015.09.034.
76. Kelsey M. Hallinen, Ross Dempsey, Monika Scholz, Xinwei Yu, Ashley Linder, Francesco Randi, Anuj Sharma, Joshua W. Shaevitz, and Andrew M. Leifer. Decoding locomotion from population neural activity in moving c. elegans. *bioRxiv*, 2021. doi: 10.1101/445643.
77. Vladislav Susoy, Wesley Hung, Daniel Witvliet, Joshua E Whitener, Min Wu, Brett J Graham, Mei Zhen, Vivek Venkatachalam, and Aravinthan DT Samuel. Natural sensory context drives diverse brain-wide activity during c. elegans mating. *bioRxiv*, 2020.
78. Daniel J. Dickinson and Bob Goldstein. CRISPR-based methods for caenorhabditis elegans genome engineering. *Genetics*, 202(3):885–901, 2016. ISSN 19432631. doi: 10.1534/genetics.115.182162.
79. Han Wang, Jonathan Liu, Shahla Gharib, Cynthia M. Chai, Erich M. Schwarz, Navin Pokala, and Paul W. Sternberg. CGAL, a temperature-robust GAL4-UAS system for Caenorhabditis elegans. *Nat. Methods*, 14(2):145–148, 2017. ISSN 15487105. doi: 10.1038/nmeth.4109.
80. Dirk R. Albrecht and Cornelia I. Bargmann. High-content behavioral analysis of Caenorhabditis elegans in precise spatiotemporal chemical environments. *Nat. Methods*, 8(7):599–606, 2011. ISSN 15487091. doi: 10.1038/nmeth.1630.
81. Jeffrey P. Nguyen, Ashley N. Linder, George S. Plummer, Joshua W. Shaevitz, and Andrew M. Leifer. Automatically tracking neurons in a moving and deforming brain. *PLOS Computational Biology*, 13(5):1–19, 05 2017. doi: 10.1371/journal.pcbi.1005517.
82. Vivek Venkatachalam, Ni Ji, Xian Wang, Christopher Clark, James Kameron Mitchell, Mason Klein, Christopher J. Tabone, Jeremy Florman, Hongfei Ji, Joel Greenwood, Andrew D. Chisholm, Jagan Srinivasan, Mark Alkema, Mei Zhen, and Aravinthan D. T. Samuel. Pan-neuronal imaging in roaming Caenorhabditis elegans. *Proceedings of the National Academy of Sciences of the United States of America*, 113(8):E1082–8, feb 2016. ISSN 1091-6490. doi: 10.1073/pnas.1507109113.
83. Butcher RA, Fujita M, Schroeder FC, and Clardy J. Small-molecule pheromones that control dauer development in caenorhabditis elegans. *Nature chemical biology*, 2007.
84. John D Storey. A direct approach to false discovery rates. *J. R. Statist. Soc. B*, 64:479–498, 2002.
85. Emmanuel Candès and Benjamin Recht. Exact matrix completion via convex optimization. *Commun. ACM*, 55(6):111–119, 2012. ISSN 00010782. doi: 10.1145/2184319.2184343.
86. Luong Trung Nguyen, Junhan Kim, and Byonghyo Shim. Low-Rank Matrix Completion: A Contemporary Survey. *IEEE Access*, 7:94215–94237, 2019. ISSN 21693536. doi: 10.1109/ACCESS.2019.2928130.
87. Jicong Fan, Lijun Ding, Yudong Chen, and Madeleine Udell. Factor group-sparse regularization for efficient low-rank matrix recovery. *Advances in Neural Information Processing Systems*, 32, 2019.
88. Melissa Linkert, Curtis T. Rueden, Chris Allan, Jean Marie Burel, Will Moore, Andrew Patterson, Brian Loranger, Josh Moore, Carlos Neves, Donald MacDonald, Aleksandra Tarkowska, Caitlin Sticco, Emma Hill, Mike Rossner, Kevin W. Eliceiri, and Jason R. Swedlow. Metadata matters: Access to image data in the real world, may 2010. ISSN 00219525.
89. Peter Kovesi. Good Colour Maps : How to Design Them. *arXiv*, pages 1–42, 2015.

Supplement

Supplemental methods

A: Identifying neurons in the ZM10104 strain

The ZM10104 strain used in this experiment expresses two fluorescent proteins: GCaMP6s driven by the *ift-20* promoter, and wCherry driven by *gpc-1*. GCaMP6s expression was localized to neuronal nuclei to minimize spatial overlap of neighboring neurons, and to make identification of neurons easier. The promoter *ift-20* drives GCaMP expression in all ciliated sensory neurons. Our neurons of interest, the chemosensory neurons, lie in the lateral ganglia, but note that this promoter drives expression in cells outside of the lateral ganglia. The wCherry landmark is expressed in the cytoplasm of AFD, AWB, ASI, ASE, AWC, and ASJ. Note that it also is expressed in RIB, a neuron which is not labeled with GCaMP.

Relative positions are given in the orientation in **Figure S1**, with the nose to the left, the tail to the right, dorsal top, and ventral bottom. Relative positions should be interpreted as “usually but not always," unless otherwise noted. Also note that overly compressing an animal in any direction will distort the relative positions. Before identifying neurons, it is important to identify the orientation of the animal in the recording by figuring out where the dorsal-ventral (DV) plane lies. This is most easily done by identifying the plane of bilateral symmetry. Once you have oriented yourself, you can begin the neuron identification process.

The easiest neurons to immediately identify in this strain are ASH, ASJ, and the anterior “triplet" of ASK, ADL, ASI. It is often effective to identify these neurons first, then work on the other neurons using the color landmarks and process of elimination. AWC and ASE should usually be in the neighborhood of ASH, and the four neurons AWA, AWB, ADF, and ASG are between ASH and the anterior triplet. These four neurons occasionally overlap. To avoid signal mixing, overlapping neurons were exluded from the dataset. For each odorant condition, neuronal identification was carried out independently by at least two individuals.

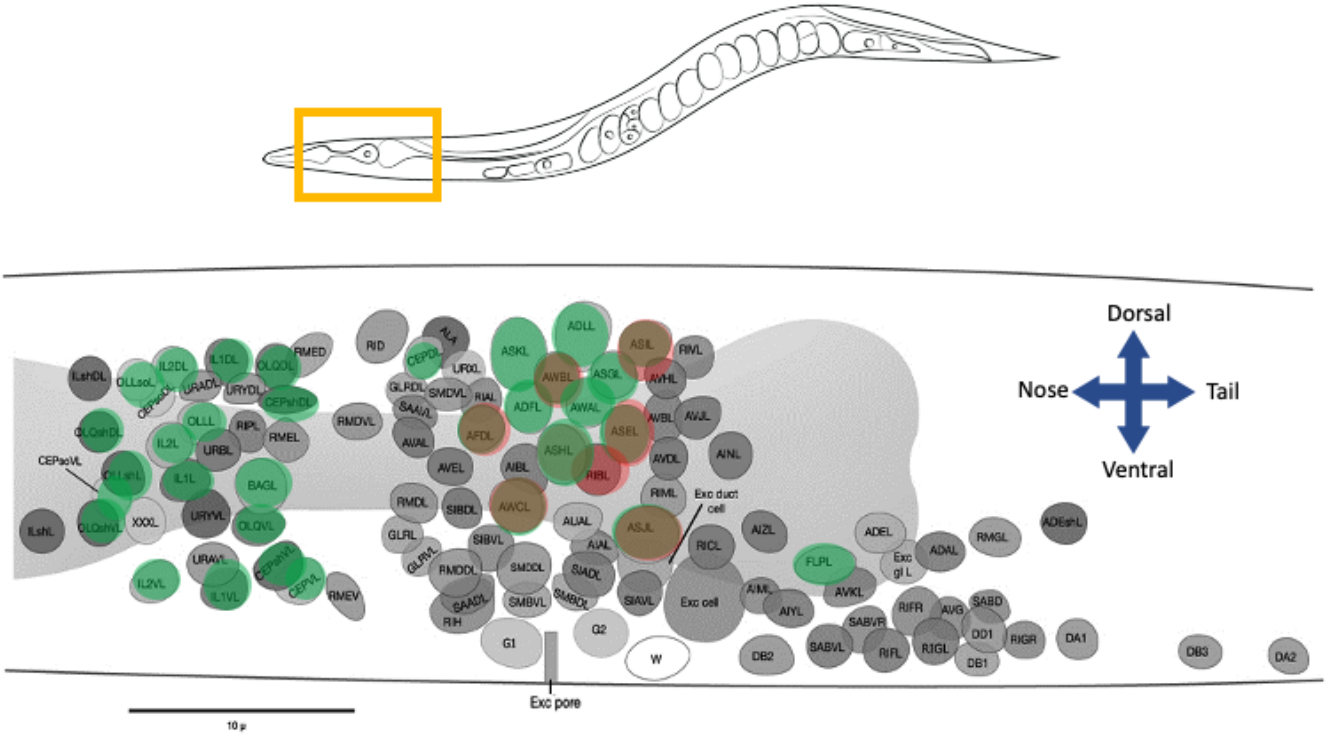

Figure S1. Identifying neurons in the ZM10104 strain. The *ift-20* promoter drives GCaMP expression in the nuclei of ciliated sensory neurons. The nuclei of the chemosensory neurons are all posterior to the nerve ring. A red landmark is provided by cytoplasmic expression of wCherry in the neurons AFD, AWB, ASI, ASE, AWC, and ASJ. Underlying *C. elegans* figure adapted from the digital version of White et al. 1986 (Wormbook)(25).

Criteria for identifying each neuron class

Neuron	Color(s)	Relative Position	Notes
ASK	green	leftmost of the anterior triplet	large. do not confuse with URX, a small oblong neuron above ASK
ADL	green	part of the anterior triplet	larger than ASI
ASI	green & red	part of the anterior triplet	use color to distinguish from ADL
ASH	green & red	left of ASE, below AWA	bright, circular
ASE	green & red	right of ASH	smaller than ASH
AWC	green & red	variable. below ASH but can be to the left, directly below, or to the right	often oblong in shape
ASJ	green & red	tail end of the ganglion, bottom left	distance from AWC can vary
AWA	green	variable. usually above ASH	smaller than ASH, circular
AWB	green & red	position variable, usually directly below the anterior triplet	small, dim, a bit oblong. use color to identify
ADF	green	usually left of AWA, AWB	dim
ASG	green	usually right of AWA, AWB	small, circular

To minimize the chances of incorrect identification, neuronal IDs for each odorant condition were reviewed by at least two individuals, and ambiguous neurons were omitted from the analyzed datasets.

B: List of odorants

Odorant	Chemical class	Behavioral valence (low conc.)
1-pentanol	alcohol	attractive
1-hexanol	alcohol	attractive
1-heptanol	alcohol	repulsive
1-octanol	alcohol	repulsive
1-nonanol	alcohol	repulsive
isoamyl alcohol	alcohol	attractive
geraniol	alcohol	attractive
benzaldehyde	aromatic	attractive
methyl salicylate	aromatic	attractive
ethyl acetate	ester	attractive
ethyl butyrate	ester	attractive
ethyl heptanoate	ester	attractive
pentyl acetate	ester	attractive
butyl butyrate	ester	attractive
diacetyl	ketone	attractive
2-butanone	ketone	attractive
2-heptanone	ketone	attractive
2-nonanone	ketone	repulsive
2,3-pentanedione	ketone	attractive
2,5-dimethylpyrazine	pyrazine	attractive
2-methylpyrazine	pyrazine	attractive
2-isobutylthiazole	thiazole	attractive
2,4,5-trimethylthiazole	thiazole	attractive

C: Neuron tracking and signal extraction

To segment the neuronal nuclei in each recording, we built a GUI which allows users to navigate each 3D landmark image and click to add or remove neuron centers (41, 82). This GUI allows the user to toggle between multiple fluorescent channels and a maximum projection, allowing the user to take advantage of any fluorescent landmark labels in the strain. Complete labeling of all neuron centers is only necessary once for a given animal, even if multiple recordings have been made. The user then labels a small handful of widely spaced neurons (4-8) in the first frame of the activity recording. This small number of labeled neurons helps the tracking algorithm to compensate for any global motion or distortion that may have occurred in the animal between the landmark volume and the activity movie. In addition to segmentation, the GUI allows neurons to be manually identified. The names the user applies are then associated with the activity traces of those neurons.

Neighborhood correlation tracking of individual neurons

While the entire brain of the worm can distort significantly across large distances, the neighborhood immediately surrounding a neuronal nucleus of interest tends to remain consistent, with little local deformation. Our image registration strategy relies on this fact. Instead of attempting to identify neuron centers in every frame, we try to match the neighborhood surrounding the neuron center in the first frame to the most similar neighborhood in the following frame. We then return the center of the new neighborhood as the position of the neuron center in the next frame.

We first employ this approach to map the neuron centers identified in the high-resolution landmark volume during the segmentation step onto the first frame of the activity movie, which is captured at a lower resolution. We then proceed to compare each frame of the movie to the next. The neighborhood correlation comparison is made independently for each neuron. While we lose some information about local deformations by not integrating information about how neighboring neurons are moving, we gain the ability to run the tracking of each neuron in a dataset as a parallel process, dramatically decreasing runtime. This also prevents a mistake in tracking one neuron from propagating to other nearby neurons. We run the tracking on a down-sampled version of the activity movie, also to improve runtime.

For a given neuron center, the tracking algorithm goes through the following steps:

1. Given the position of the given neuron center in the current frame, $n_t = (x_t, y_t, z_t)$, we identify the neuron's local 3D neighborhood N_t in that frame, the volume with dimensions $2a * 2b * 2c$, in the region spanned by $[x_t - a, x_t + a]$, $[y_t - b, y_t + b]$, and $[z_t - c, z_t + c]$.

2. We identify the naive center in frame $t+1$, from where we begin our search for the neighborhood most similar to N_t. For the first frame of the movie, this point is adjusted by a distance-weighted average of the manually labeled neurons: $n'_{t+1} = (x_t + \Delta\Sigma w x^i, y_t + \Delta\Sigma w y^i, z_t + \Delta\Sigma w z^i)$. For any other frame, we simply take the naive center as the center of the previous frame, $n'_{t+1} = n_t = (x_t, y_t, z_t)$.

3. Starting from the naive center n'_{t+1}, we perform image registration between the maximum intensity projections in x, y, and z of putative neighborhood N'_{t+1} and the previous neighborhood N_t, computing the pairwise correlation of these images. We then repeat this process, moving the putative center n'_{t+1} by 1 pixel per iteration until one of the following occurs:

   (a) The algorithm finds a putative neighborhood N'_{t+1} whose correlation with N_t exceeds the confidence threshold C (usually set at above 90%). This putative neighborhood is then defined as N_{t+1}.

   (b) The algorithm tests all putative neighborhoods within a maximum search radius $r_{\max}$ of the naive center n'_{t+1}, but failed to find a putative neighborhood whose correlation exceeds the confidence threshold C. The algorithm then returns the putative neighborhood with the highest correlation with N_t as N_{t+1}.

   (c) If no neighborhood is found with a correlation exceeding a minimum value, the neuron is considered lost in frame $t+1$, likely either due to motion taking the neuron outside the region of interest. No center is reported, and the last reported neighborhood N_t is used as the basis of comparison for following frames ($t+2, t+3$, etc.).

4. The center of neighborhood N_{t+1} is defined as the neuron center in this frame, n_{t+1}.

5. Repeat until the end of the activity movie is reached.

We can optimize the tracking parameters such as neighborhood size (a, b, c), maximum search radius $r_{\max}$, and confidence threshold C for both accuracy and speed for different imaging conditions.

Extracting calcium dynamics

To extract calcium signals, we first map the positions of each tracked neuron center back onto the original-resolution volumetric images. We then extract fluorescence values from these images. We identify a small volume around each neuron center, containing voxels whose fluorescence will be assigned to the neuron. This volume is set as 2 µm x 2 µm x 3 µm for our data. We compute the mean of the 10 brightest pixels within this volume to extract a raw fluorescence trace $F_r(t)$. We then account for photobleaching by exponential detrending, giving us a clean fluorescence activity trace $F(t)$. We then identify the background fluorescence F_0 for each neuron, and report normalized neuron activity $\Delta F/F_0$.

Manual proofreading of traces

The manual proofreading step gives us the opportunity to improve the quality of the data by removing neurons which have been mistracked, adjust the computer-determined baseline fluorescence F_0, and to correct or add nuclear IDs. It also enabled us to remove traces which were contaminated by the signals of neighboring neurons. The software then compiles all of the processed traces for a given individual into a single data structure.

D: Imputing missing single-trial responses

Across trials of all neurons and all conditions, about 20% of the neuron responses were either not captured, or excluded due to tracking mistakes or signal contamination issues. To perform single-trial discrimination analysis in the (N-dimensional) neural response space, we first had to fill these missing data points in a reasonable and biologically motivated way.

For a given odorant and M trials, the peak responses of the $N = 11$ sensory neurons can be compiled in a matrix $R \in \mathbb{R}^{N\times M}$. Without any assumptions for the values R, it is impossible to infer the missing data. Fortunately, due to the intrinsic correlation between the responses of different olfactory neurons, the full response matrix R is low rank (as indicated by the PCA of neural responses). We can use this low-rank information to recover the missing entries: "matrix completion" algorithms can solve this problem very efficiently (85, 86).

To verify that matrix completion can indeed recover the missing entries faithfully, we performed a holdout evaluation. For the response matrix to each odor, we performed matrix completion after randomly removing 20 entries ($x_i, i = 1, \cdots, 20$). The imputed matrix is denoted as X^*. We then calculated the Pearson correlation coefficient ρ between the estimated entries x_i^* with the true entries x_i. The average value of ρ is around 0.7 (**Figure**). We used the MATLAB code provided in (87) with default parameters for matrix completion (`https://github.com/udellgroup/Codes-of-FGSR-for-effecient-low-rank-matrix-recovery`). Specifically, we chose an algorithm based on minimization of the nuclear norm `MC_Nulcear_IALM`.

E: Computational methods for discriminability quantification

For binary classification of all odorant pairs, we used linear regression and a simple SVM (linear or Gaussian kernel). To decode odor identity from the entire single-trial dataset, we built a multi-class classifier. We concatenate all of the single-trial responses of the 23 odorants at high concentration. Each trial is an 11-dimensional point, one dimension for every neuron class. Each point has an associated label indicating the odorant identity. This data set was randomly divided into 10 parts, 9 of which are used as a training set (90%) and one which is used as a validation set (10%).

We used the MATLAB function `fitcecoc` to fit a multi-class model which supports both SVM and other classifiers. Mechanistically, this method reduces the problem of overall classification into a sequence of binary classification problems. The performance was quantified by the classification error, estimated using the `crossval` function. The confusion matrix was generated using the functions `kfoldPredict` and `confusionchart`. The training is repeated 10 times, using each of the 10 parts of the datasets as the validation set, and the results were compiled.

For the *in silico* knockouts, we removed neurons from the training dataset, resulting, for example in 10-dimensional responses when one neuron was removed. We trained the multi-class classifier as above.

F: Statistics, code, and software

All statistical computations and image analysis code were written and run in MATLAB using standard toolboxes, with the exception of the OME Bio-Formats API (used to read Nikon ND2 file formats) (88) and CET Perceptually Uniform Color Maps (89).

Supplemental figures

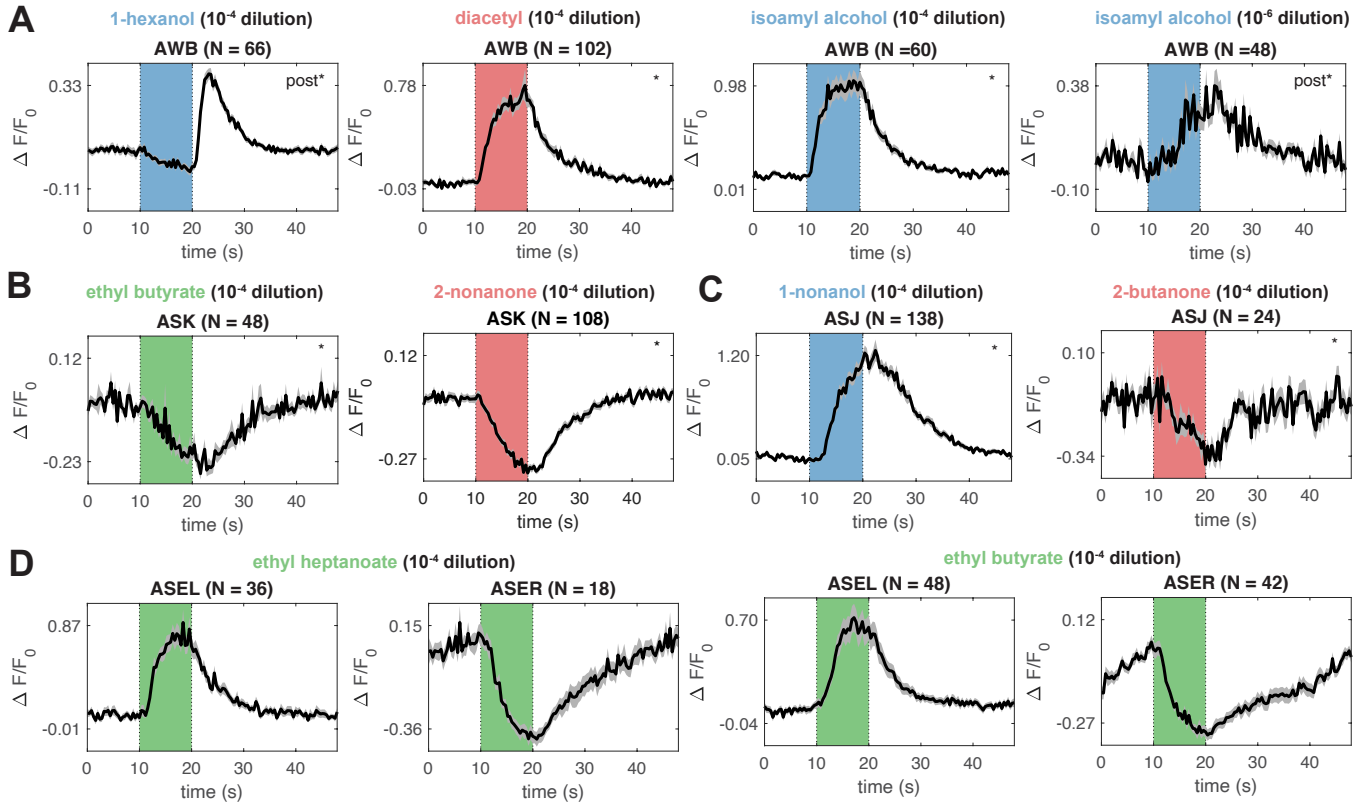

Figure S2. Single neuron response observations. (A) AWB is an OFF response for most stimuli, such as 1-hexanol, but is occasionally an ON response, as is the case for high concentration diacetyl. High concentration isoamyl alcohol elicits an ON response from AWB, but low concentration isoamyl alcohol elicits an OFF response. This has been previously observed in Yoshida et al., 2012 (35). **(B)** We observe inhibitory responses to some odorants in ASK. **(C)** ASJ has an excitatory response to some odorants, such as 1-nonanol, but has an inhibitory response to 2-butanone. **(D)** We observe L/R asymmetries in ASE in response to several odorants, such as ethyl heptanoate and butyl butyrate.

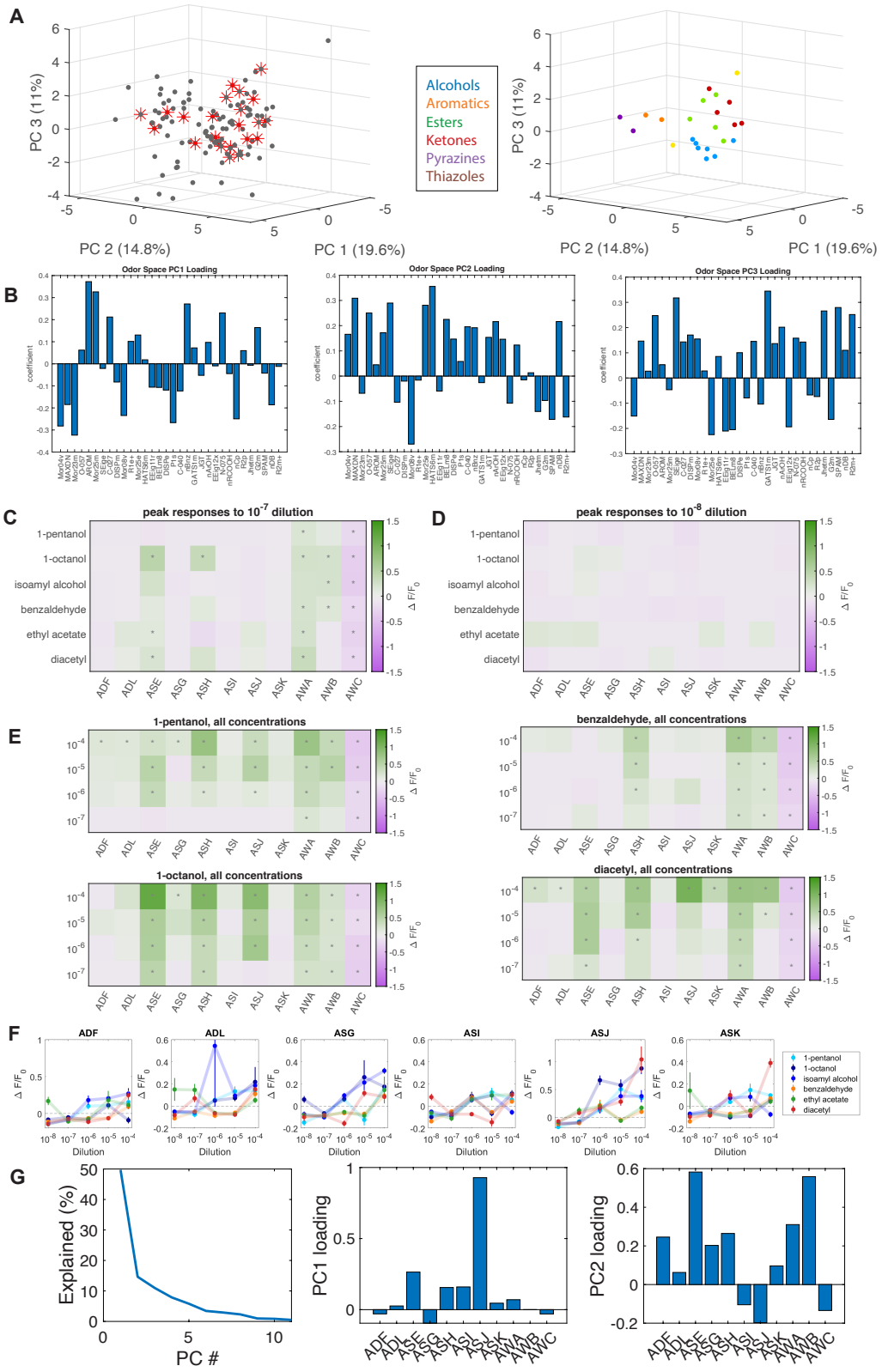

Figure S3. Supplemental panels for Figure 2. (A) An odor space constructed from the molecular descriptors of 122 odorants (gray) previously studied in *C. elegans*. We selected for our experiments a panel of 23 odorants (red) which span the odor space (left). On the right, these 23 odorants are presented in odor space colored by their chemical class. **(B)** The molecular descriptor loadings of the first 3 principal components of the *C. elegans* odor space, plotted on the same axes. The leading components of PC 1 are measures of aromaticity, and the leading components of PC2 are measures of electronegativity. Peak responses for six odors tested at **(C)** 10^{-7} and **(D)** 10^{-8} dilutions. Statistically significant responses ($q \leq 0.01$) are indicated with stars—no significant activity was observed at the lowest tested dilution. **(E)** Compiled responses to three representative odorants at multiple concentrations (1-pentanol, 1-nonanol, and benzaldehyde) show similar neural responses across concentration. The magnitude of neuron responses generally increases with increasing concentration, and for some conditions, additional neurons are recruited at high concentration. **(F)** Dose responses for the six sensory neurons not printed in **Figure 2D**. **(G)** The variance explained and the loadings of the first two principal components of the standardized average peak neural response PC space in **Figure 2F**.

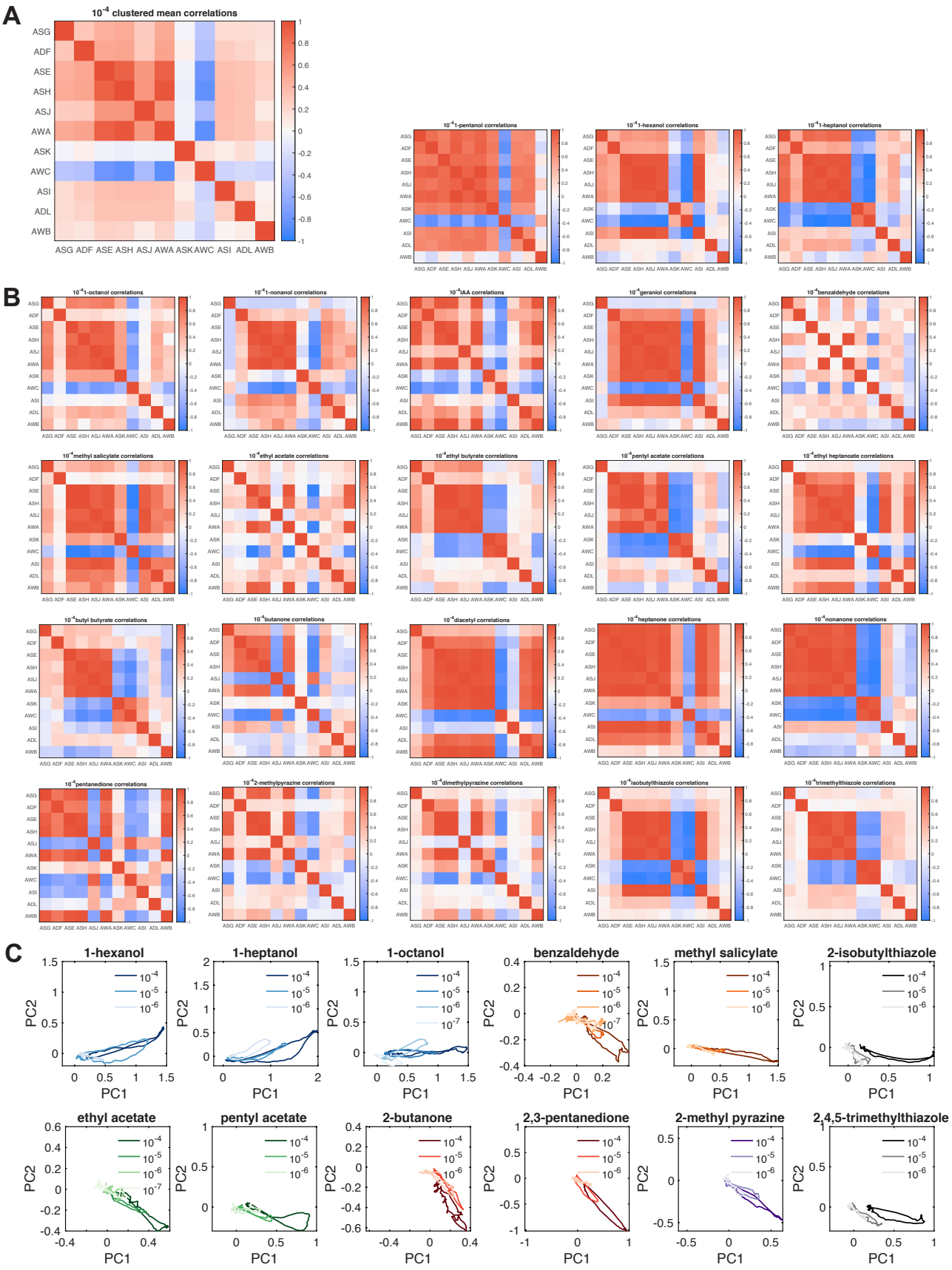

Figure S4. Time trace correlations and phase trajectory analyses. (A) Average time trace correlation map of the 11 chemosensory neuron responses across all 23 odorants. **(B)** Average correlation maps of responses to all 23 odorants at high concentration, plotted on the same axes, show diverse response dynamics. **(C)** Phase trajectory plots of average neural activity for select odorants, all plotted in a common PC space. The shade of each color indicates concentration, with low concentration indicated by a light shade and high concentration indicated by a dark shade. Different concentrations of the same odorant tend to generate similar trajectories.

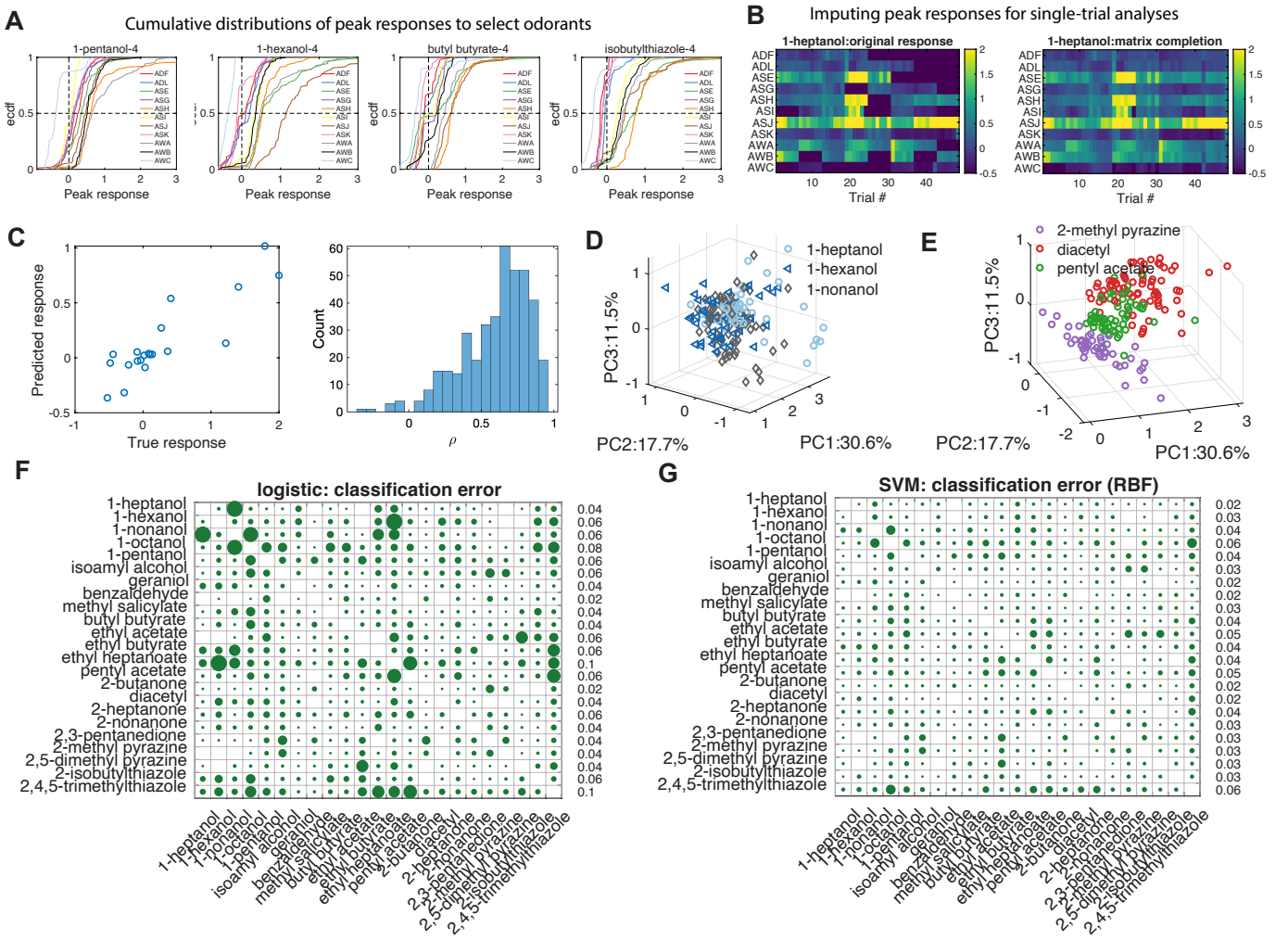

Figure S5. Supplemental panels for Figure 3. (A) Cumulative distributions of peak responses of every neuron (four exemplar odorants shown). **(B)** Signals were not always captured from all 22 chemosensory neurons in every trial. We used a matrix completion algorithm to impute these missing data points. Here are shown the peak responses all chemosensory neurons to 1-heptanol in different trials, with missing responses in black (left) and after matrix completion (right). **(C)** *Left*: To quantify the performance matrix completion, we randomly removed 20 measured responses (true response) and compared the imputed values from matrix completion (predicted responses).*Right*: The histogram of Pearson's correlation coefficient between true responses and predicted responses. For each response matrix, we repeated 5 times. **(D/E)** Representations of single-trial peak neural responses to sets of **(D)** three similar and **(E)** three dissimilar odorants. These data are plotted in a PC space constructed from the individual trial responses to all odorants in the dataset. **(D)** We see that three similar odorants, the straight-chain alcohols 1-hexanol, 1-heptanol, and 1-nonanol, have more similar neural representations. **(E)** In contrast, three odorants of three distinct chemical classes, 2-methylpyrazine (a pyrazine), diacetyl (a ketone), and pentyl acetate (an ester), have more easily separable neural representations. Binary classification of all odorant pairs by **(F)** logistic regression and **(G)** SVM. Both methods return very low classification errors, demonstrating that the single-trial peak responses of any two odorants are linearly separable. Shown here are classification error heatmaps at high concentration (10^{-4} dilution), for which the average classification error is 0.055 for the logistic regression and 0.035 for the SVM.

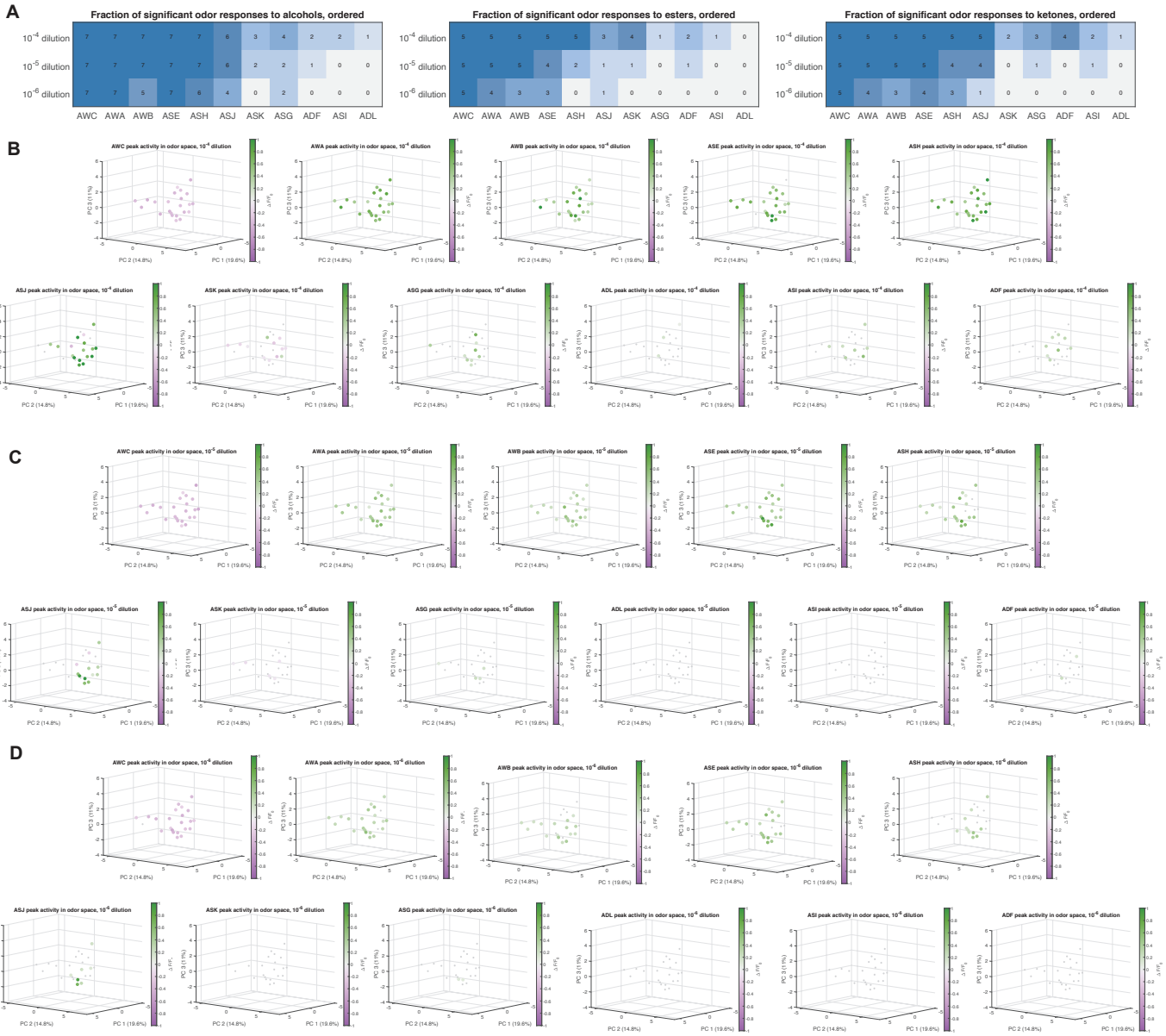

Figure S6. Average peak responses plotted in odor space. (A) The fraction of significant odor responses to three chemical groups: alcohols, esters, and ketones. Average peak responses of each of the 11 chemosensory neuron classes plotted in odor space (**Figure S3A**), at **(B)** high odorant concentration (10^{-4}), **(C)** medium odorant concentration (10^{-5}), and **(D)** low odorant concentration (10^{-6}).